5-2022

Feasibility Assessment on Use of Proximal Geophysical Sensors to Support Precision Management

Sophia M. Becker
University of Nebraska-Lincoln, sbecker14@huskers.unl.edu

FEASIBILITY ASSESSMENT ON USE OF PROXIMAL GEOPHYSICAL SENSORS TO SUPPORT PRECISION MANAGEMENT

by

Sophia M. Becker

A THESIS

Presented to the Faculty of

The Graduate College at the University of Nebraska

In Partial Fulfillment of Requirements

For the Degree of Master of Sciences

Major: Natural Resource Sciences

Under the Supervision of Professor Trenton E. Franz

Lincoln, Nebraska

May, 2022

FEASIBILITY ASSESSMENT ON USE OF PROXIMAL GEOPHYSICAL SENSORS TO SUPPORT PRECISION MANAGEMENT

Sophia M. Becker, M.S.

University of Nebraska, 2022

Advisor: Trenton E. Franz

Soil property maps provide information for field management activities such as irrigation, fertilization, and seeding. Many on-the-go proximal geophysical sensors have been developed in recent decades that can help map agricultural fields without dense soil sampling. To utilize these technologies most profitably in precision management, scientists and precision agriculture dealers must better understand sensors' performances in given field conditions and the economic value of different proximal soil sensing methods.

Chapter two reports the study that was conducted at three sites in North Dakota, United States to strengthen understanding of the usefulness of different proximal geophysical data types in agricultural contexts of varying pedology. This study hypothesizes that electro-magnetic induction (EMI), gamma-ray sensor (GRS), cosmic-ray neutron sensor (CRNS), and elevation data layers are all useful in multiple linear regression (MLR) predictions of soil properties that meet expert criteria at three agricultural sites. In addition to geophysical data collection with vehicle-mounted sensors, 15 soil samples were collected at each site and analyzed for nine soil properties of interest. A set of model training data was compiled by pairing the sampled soil

property measurements with the nearest geophysical data. Eleven models passed expert-defined uncertainty criteria at site 1, 16 passed at site 2, and 14 passed at site 3. Electrical conductivity, organic matter, available water holding capacity, silt, and clay were predicted at site 1 with an $R^2_{pred} > .50$ and acceptable RMSEP. Bulk density, organic matter, available water capacity, silt, and clay were predicted with $R^2_{pred} > .50$ and acceptable RMSEP at site 2. At site 3, no soil properties were predicted with acceptable RMSEP and an $R^2_{pred} > .50$. These results confirm feasibility of our method, and the authors recommend the prioritization of EMI data collection if geophysical data collection is limited to a single mapping effort and calibration soil samples are few.

Strategies for addressing the remaining needs for better prediction of sensor performance and evaluation of sensing methods' economic value are discussed in chapter three. Several potential methods for future research from the literature are summarized that can advance understanding of sensors' best use, sophisticated cost-benefit analysis, and soil sampling optimization.

ACKNOWLEDGEMENTS

I would like to first thank the School of Natural Resources at the University of Nebraska for supporting me with a Graduate Teaching Assistantship throughout my master's degree. The financial freedom to complete a master's degree and the opportunity to learn more about teaching have been instrumental in my career development.

The research presented is a result of a joint study by USDA-NRCS North Dakota (under agreement #NR206633XXXXC001), North Dakota State University, and the University of Nebraska-Lincoln on irrigation water management and variable rate irrigation technologies; and was partially supported by the North Dakota Agricultural Experiment Station. I am thankful for the input of Dean Steele, J. Paulo Flores, Xinhua Jia, and Thomas Scherer on my manuscript for Chapter 2. I appreciate the equipment, time, and expertise for soil sampling provided by Jordaan Thompson-Larson, Erica Althoff, and others of the USDA-NRCS staff of North Dakota. I thank Sheldon Tuscherer, Dongqing Lin, and Mathew Blum for field and laboratory support

Many thanks to my advisor, Dr. Trenton Franz, for the opportunity to learn from him and work on this project. Dr. Franz has provided good support and challenge that has grown me as a researcher and deepened my interest in hydrogeophysics. I also thank Olufemi Abimbola for his advice on my statistical methods and detailed feedback on my manuscript.

Thank you to my committee members, Dr. Daran Rudnick and Dr. Jesse Korus, for their investment in this thesis and my degree progress.

I thank the Department of Geology and Environmental Science at Wheaton College for first fostering my love for geoscience and instilling me with the confidence and skills to pursue graduate education.

Finally, thank you to Mom, Dad, David, Cole, Aliza, and Ike for providing much-needed encouragement and laughter over the past two years. I am also grateful for the love and support of my grandparents and friends throughout this journey.

GRANT ACKNOWLEDGEMENTS

I acknowledge the support from USDA National Institute of Food and Agriculture Foundational Program Cyber-physical systems (2019-67021-29312). T.E.F. and D.D.S acknowledge the financial support of the USDA National Institute of Food and Agriculture, Hatch project #s 1009760 and ND0140, respectively. Financial support was provided by the Joint FAO/IAEA Programme of Nuclear Techniques in Food and Agriculture through the Coordinated Research Project (CRP) D1.20.14 Enhancing agricultural resilience and water security using Cosmic-Ray Neutron Sensor (2019–2024).

Table of Contents

List of Figures

List of Tables

List of Abbreviations

BD	Bulk Density
CEC	Cation Exchange Capacity
CRNS	Cosmic-ray Neutron Sensor
EC	Electrical Conductivity
ECaD	Deep Apparent Electrical Conductivity
ECaS	Shallow Apparent Electrical Conductivity
ECaSDR	Ratio of Shallow to Deep Apparent Electrical Conductivity
EMI	Electromagnetic Induction
GRS	Gamma-ray Sensor
NC	Neutron Counts
OM	Organic Matter
SWC	Soil Water Content estimated from cosmic-ray neutron sensor
ThUR	Ratio of Thorium to Uranium Concentration

CHAPTER 1

INTRODUCTION TO PROXIMAL SENSING IN PRECISION MANAGEMENT

1.1 Introduction

Proximal sensing "refers to field-based techniques that can be used to measure soil properties from a distance of approximately less than 2 m above the soil surface" (Viscarra Rossel et al., 2009), and utilizes technology with measurement scales between the point and remote sensing scales. On-the-go proximal sensors can be hand-held or mounted on vehicles to gather geo-referenced information about the earth's surface that can be compiled into various maps (Adamchuk, Hummel, et al., 2004a). Soil maps are often important information for optimizing field management. This review examines research from the past 20 years on proximal sensors used in soil mapping. Objectives are to 1) examine the use of data fusion in soil mapping and precision management research and 2) identify remaining needs in precision management soil mapping.

1.2 Precision management

Modern precision agriculture was born from the introduction of publicly available Global Positioning Systems in the 1980's (Evett et al., 2020), which allowed farmers to variably manage different geo-referenced regions within their fields. Precision agriculture includes a wide range of technologies and software that are each relevant to different settings. Automated farming equipment is beginning to emerge - such as certain herbicide sprayers - that can make on-the fly adjustments to a farming activity. Other precision management activities rely on prior knowledge of static properties (Evett et al., 2020).

Soil maps are an example of a static precision management tool which can be translated into prescription maps for application of fertilizer, compost, lime, or irrigation water (van Egmond et al., 2010). Seeding rate and variety can also be prescribed based on soil maps (Schimmelpfennig, 2016).

According to a 2017 survey of 209 precision dealers, grid or zone soil sampling services were profitable for 68% of dealers (Lowenberg-DeBoer, 2017). Although it's difficult to explicitly define its benefits across the board, soil mapping was one of the more profitable precision agriculture services, behind variable rate technologies for fertilizer application and lime application (Lowenberg-DeBoer, 2017). Soil mapping will always remain a prerequisite for implementing profitable variable rate technologies.

Some of the soil properties of interest in soil mapping for precision management are clay content, cation exchange capacity (CEC), pH, organic matter (OM), and bulk density. These are used to prescribe seeding, fertilizer, tillage, and irrigation management (Schimmelpfennig, 2016; van Egmond et al., 2010). Texture informs seeding management and influences available water capacity (AWC); CEC indicates overall fertility and soil structural resistance to tillage through shrink-swell capacity (Taylor et al., 2010; Triantafilis & Lesch, 2005); and pH maps show liming requirements (van Egmond et al., 2010). OM may be used to prescribe compost and also influences AWC. Bulk density gives information on compaction risk and preferred tillage settings (van Egmond et al., 2010). AWC directly impacts irrigation management (Lo et al., 2016).

As the driving knowledge for multiple variable rate technologies, any improvement in the accessibility and accuracy of soil mapping is pertinent to precision management. Predictive soil mapping seeks to attain greater accessibility and accuracy

over interpolation of numerous soil samples by supplementing soil core samples with covariate data from less labor-intense sources. When soil property predictions incorporate covariate data, less soil core samples can be collected, and more meaningful spatial variability can be captured between soil sample locations. For instance, Gibson and Franz (2018) were able to reduce soil sampling to only 5 samples per 65 ha using repeat hydrogeophysical surveys for mapping soil hydraulic properties. The goal of precision management in predictive soil mapping is to gain relevant soil property information at minimal time, labor, and economic costs. This can be achieved when a farmer captures an amount of sub-field variation needed to make management decisions while simultaneously minimizing economic and temporal costs of soil core sampling. Collection and analysis costs of covariate data must be low enough to be a beneficial trade-off with soil core sampling.

1.3 Proximal sensors

Although laboratory analysis, point sensors, and remote sensing can provide predictive data, this review focuses on proximal sensors. Proximal sensing technologies that have been used in agricultural contexts include electromagnetic induction (EMI), ground-penetrating radar (GPR), visible and near-infrared diffuse reflectance (VIS-NIR), gamma-ray spectroscopy, magnetic susceptibility, X-ray fluorescence; and cosmic-ray neutron sensing (CRNS) (Gibson & Franz, 2018; Grunwald et al., 2015). Each of these technologies have different best-uses since they respond to different environmental conditions at time of data collection and have different measurement volumes. GPR provides three-dimensional data and can effectively locate structure changes within the

soil profile (Castrignanò et al., 2018). VIS-NIR has been correlated with a large variety of soil properties, especially clay content and soil organic carbon (Grunwald et al., 2015; Viscarra Rossel et al., 2009; Zhang et al., 2020). Magnetic susceptibility can estimate the soil concentration of iron minerals, as well as soil drainage class (Grunwald et al., 2015). X-ray fluorescence is used to quantify the elemental composition or particle size of soil in the field or laboratory (Zhu et al., 2011). While GPR, VIS-NIR, magnetic susceptibility, X-ray fluorescence are valuable tools in proximal soil sensing, this review focuses on EMI, gamma-ray spectroscopy, and cosmic-ray neutron sensing because they were employed in the geophysical surveys conducted in Chapter 2. The role of elevation information in predictive soil mapping will also be reviewed even though it is not strictly obtained by proximal sensors but is widely available at high resolutions.

EMI measures apparent bulk electrical conductivity of the subsurface by transmitting electromagnetic soundings and then detecting the strength of an induced secondary electromagnetic field. The primary field originates from coils in the sensor's transmitter, and the electric current induced in the ground by the sensor's electromagnetic field produces the secondary electromagnetic field that is detected by the sensor's receivers (Doolittle & Brevik, 2014). Different spacing and orientations of the transmitter – receiver pairs within the sensor allow simultaneous measurement of multiple distinct exploration depths. In proximal soil sensing applications, the exploration depths are in the range of 0.4 to 6.0 m (Doolittle & Brevik, 2014). EMI is useful for estimation of salinity, depth of soil profile, clay content, and volumetric water content (A. McBratney et al., 2005). However, EMI is only able to predict each of these properties in specific salinity, soil depth, and soil type conditions. For instance, EMI cannot distinguish between sandy

soils and cemented gravel layers, so another data source must be incorporated in order to obtain soil depth in sandy soil overlying gravel (Castrignanò et al., 2012; Wong et al., 2009).

The gamma-ray sensor (GRS) consists of a scintillation crystal of NaI or CsI, into which gamma-ray photons emitted by radioactive decay collide. The collisions of a photon with the atoms in the crystal eventually emit photo electrons of the same combined kinetic energy as the original gamma-ray photon. A spectrum of detected energy is constructed for every collection interval. Measurement periods in proximal sensing applications typically range from one second to 15 minutes per spectra, depending on the detection efficiency of the scintillation crystal and the desired counting statistics (Baldoncini et al., 2019; Dierke & Werban, 2013; van Egmond et al., 2010). By analyzing the gamma-ray spectra with the full-spectrum analysis (FSA) method (Caciolli et al., 2012; Hendriks et al., 2001), activity concentrations of ^{40}K, ^{232}U, ^{238}Th, and ^{137}Cs can be estimated. ^{40}K and ^{137}Cs are estimated directly, but ^{238}U and ^{232}Th are estimated by the detection of gamma radiation emitted by the daughter products in each of their decay series, especially ^{214}Bi (^{238}U) and ^{208}Tl (^{232}Th). Radon (^{222}R) is another daughter product of ^{238}U that emits gamma-rays (IAEA, 2003).

Since gamma radiation is correlated to the concentration of ^{40}K, ^{238}U, and ^{232}Th in the soil, it can provide information about mineralogy and parent material. In addition to soil genesis, detected radiation is influenced by other soil physical and chemical properties such as soil water content, texture, organic matter, and pH (Carroll, 1981; Dierke & Werban, 2013). The inverse relationship between soil water content and detected gamma-radiation is due to signal attenuation by water. Typically, the more water

present in the soil, the less gamma radiation detected. Given that the gamma-radiation signal is attenuated by all hydrogen pools, biomass and other hydrogen sources must also be accounted for in analysis (Baldoncini et al., 2019). Rainfall and soil moisture dynamics can complicate the ^{238}U signal due to the radiation released by radon, a gaseous daughter product of ^{238}U. Atmospheric radon is brought down by rain through mechanisms termed rainout and washout, and on a much smaller scale is also trapped and released within the soil pores as water content changes (Bottardi et al., 2020; Grasty, 1997). The complexity in the ^{238}U signal introduced by atmospheric radon has been successfully interpreted by examining the ^{214}Pb signal (member of ^{238}U decay series directly preceding ^{214}Bi) and used as a tool to differentiate rainfall from irrigation water (Bottardi et al., 2020).

Although interest is rising in GRS capabilities for soil moisture monitoring (Baldoncini et al., 2019), prediction of clay content using gamma-ray sensing has been most common and successful in the literature overall, with multiple studies in the Netherlands, Sweden, and Australia finding that a strong relationship holds between ^{232}Th and clay (Mahmood et al., 2013; Rossel et al., 2007; Söderstrom et al., 2016; van der Klooster et al., 2011; van Egmond et al., 2010). Detected gamma radiation is related to pH because soil pH affects the solubility and resulting mobility and location of elements within the soil profile (Dierke & Werban, 2013). Some studies have found correlations between soil organic matter (or organic carbon) and gamma-radiation, but results vary from site to site and both positive and negative relationships have been reported (Dierke & Werban, 2013; Ji et al., 2019; Wong & Harper, 1999). In addition to

disequilibrium within the ^{238}U decay series, a weakness of GRS is that both gravels and clay soils usually produce a strong gamma-ray signal (Castrignanò et al., 2012).

The cosmic-ray neutron sensor (CRNS) relies on similar physics to the GRS and detects low energy (~0.25 – 1000 eV) neutrons with a gas tube. Low energy neutrons include both epithermal (10 – 1000 eV) and thermal (0 – 0.5 eV) neutrons, and different gas tube cases (i.e. shielding) detect different proportions of epithermal and thermal neutrons, which can be distinguished from one another for certain applications (Andreasen et al., 2016). Due to its abundance, atomic radius, and the energy lost per collision, H has the greatest effect on the number of cosmic-ray neutrons emitted from the soil (Andreasen et al., 2017). The greater the amount of H in the soil, the less neutrons are detected by the CRNS, and this inverse relationship is used to reliably estimate soil moisture (Zreda et al., 2008). In addition to soil moisture, additional H pools such as organic matter, biomass, snow cover, atmospheric water vapor, and structural water also affect neutron intensity (Franz et al., 2013; Zreda et al., 2012). The focus of CRNS research has been on soil water content estimation, but some roving CRNS surveys have predicted available water content and other soil hydraulic properties (Finkenbiner et al., 2019; Gibson & Franz, 2018). The CRNS may also be able to predict soil properties related to hydrogen pools beyond soil moisture, such as organic matter (Andreasen et al., 2016).

Finally, elevation data can be obtained from proximal tools such as Real-Time Kinematic (RTK) GPS and drone-mounted RGB cameras (Castrignanò et al., 2012). Remote sensing technologies such as satellites and LIDAR surveys also gather elevation data. Elevation itself is a useful explanatory variable, and digital elevation models can be

used to calculate other topographic variables of interest such as aspect and slope (Grunwald et al., 2015). Depending on the data source, digital elevation models can be obtained at resolutions as fine as less than 1 m (Jiménez-Jiménez et al., 2021; Polidori & El Hage, 2020). Soil formation, soil water content, and organic matter content are all influenced by elevation (Florinsky et al., 2002).

1.4 Data fusion

As seen in the above descriptions, each proximal sensor has different spatial scales, strengths, and weaknesses. The support volumes of CRNS, GRS, and EMI are depicted in Table 1. All are affected by sensor height and soil water content (Carroll, 1981; Köhli et al., 2015; Morris, 2009; Zreda et al., 2008). In addition to different scales, each of the data types capture unique information. The CRNS detects particles in the 0 – 10 KeV range, while the GRS detects particles in the 0 – 3 MeV range. Electrical conductivity is recorded in mS/m by the EMI sensor, which detects radiation within the broad band radio spectrum (~ 10^{-11} eV; Doolittle & Brevik, 2014). Performance of these sensing technologies for specific tasks is highly dependent upon environmental conditions. Different settings expose weaknesses in individual sensor ability to accurate capture the target variable for soil property mapping.

Table 1.1. The spatial and temporal scales of the cosmic-ray neutron sensor (CRNS), gamma-ray sensor (GRS), and electromagnetic induction sensor (EMI) are summarized for a sensor height of 1.5 m above the ground (Doolittle & Brevik, 2014; Köhli et al., 2015; van der Veeke et al., 2021; Zreda et al., 2008). Radii of the circular stationary footprint are given, and the percent of detected signal expected to originate within the given measurement volume is also provided.

Sensor	Radius (m)	Depth (m)	Signal contribution	Collection time (s)
CRNS	200	0.12 - 0.76	86 %	60
GRS	24	0.30 - 0.60	95 %	10
EMI	0.5 - 2	0.40 - 6.0	70 %	< 1

Since no single sensor can fully characterize the soil, researchers integrate information from multiple sensors in an approach termed data fusion (Grunwald et al., 2015). In data fusion, decision-making knowledge is gleaned from multiple measurement volumes and information types. Some of the studies exploring the contributions of EMI, GRS, CRNS, and elevation are summarized below.

Taylor et al. (2010) evaluated the predictive abilities of EMI, GRS, and elevation data for pH, clay content, and CEC models in Scotland. Almost all models for pH were unsatisfactory, but data fusion did improve prediction of subsoil (0.45 – 1.0 m) pH over prediction with individual sensors. Data fusion also improved prediction of topsoil clay (0 – 0.45m). Individually, the GRS was more successful for topsoil clay predictions and EMI was more successful for subsoil clay predictions. This follows the difference in sensing depths between the two sensors; 80% of the detected EMI signal originated from the top 1.1 m while the GRS response was generated from the top 0.3 – 0.6 m of the soil (Abdu et al., 2007).

In another study fusing EMI, GRS, and elevation data, Castrignanò et al. (2012) estimated crop available soil potassium and described soil variation in an agricultural field in Western Australia. Using multivariate geostatistical techniques and principal

components analysis, Castrignanò et al. found that the spatial component of the crop available soil K model was significant. Crop available soil K was accurately predicted by the gamma-ray ^{40}K signal, suggesting that GRS would be useful for precision management of K fertilizer, but the authors didn't assume that the strong relationship between the ^{40}K and crop available soil K will hold everywhere. Homogenous soil zones were identified by using the combined EMI, GRS, and elevation data, showing that the sensor data fusion allows detection of soil types that could not be clearly identified by individual sensors (e.g., sandy, sandy gravelly, sandy salt-affected, and clayey soils).

Rodrigues et al. (2015) explored what GRS relationships might hold across multiple sites, integrating EMI and GRS for more universal prediction of CEC and clay content in South Australia and Queensland. When the data from all eight study sites was integrated in a weighted principal component analysis, significant models ($p < 0.05$) were found for predictions of clay and CEC at five of the sites. The success of some of the models calibrated with data from all the sites showed some potential of moving toward universal models instead of site-specific predictions. Rodrigues et al. also determined that clay and CEC predictions were improved when using both EMI and GRS instead of just one sensor.

Ji et al. (2019) added vis-NIR into the EMI, GRS, and elevation data combination to predict soil organic matter, Ca, Mg, Al, pH, lime buffering capacity, P, and K in an agricultural field in Quebec, Canada. Partial least squares regressions was used for prediction, and Ji et al. found that predictions, which were calibrated using 56 soil samples from within the 11 ha field, were generally better when using combined information than when using individual sensors. ^{40}K and ^{232}Th had the highest relative

importance in prediction of soil organic matter. Vis-NIR and EMI had the highest relative importance in prediction of pH.

With a slightly different focus from the soil mapping studies mentioned so far, Finkenbiner et al. (2019) evaluated the potential of EMI, CRNS, elevation, and topographic wetness index to predict soil hydraulic properties. At a 53 ha field in west-central Nebraska, United States, multiple CRNS surveys were performed to capture the range of soil moisture conditions and then empirical orthogonal components were found from the repeated CRNS surveys. Predictions were made for soil water content at field capacity, soil water content at wilting point, and available water capacity with aims of developing irrigation management zones. Finkenbiner et al. did not integrate all the different data types but did combine elevation and CRNS. Compared to all of the other individual data types, the combination of elevation and CRNS performed the best, followed by CRNS alone. In a similar study, Gibson and Franz (2018) concluded that a combination of environmental covariates would likely be preferrable to prediction of soil hydraulic properties with EMI or CRNS alone.

1.5 Conclusions

Taylor et al. (2010), Castrignanò et al. (2012), Rodrigues et al. (2015), Ji et al. (2019), and Finkenbiner et al. (2019) all reported benefits of proximal sensor fusion. Although it has been established that proximal sensor fusion is generally advantageous for soil mapping, the literature lacks expansion on some key concepts. Two subjects with room for development are 1) a systematic understanding of sensor performance in specific conditions and 2) the value of proximal soil sensing to the agriculture industry.

So far, studies on proximal sensor fusion have found that success of soil property prediction varies among sites (Rodrigues Jr. et al., 2015; Wong & Harper, 1999). Both static and dynamic environmental variables alter the outcome of soil property prediction. Static environmental variables such as soil texture, parent materials, and amount of variation in a target soil property affect the correlations between soil properties and sensor data at a given site. These interactions can be better understood through theoretical consideration (Doolittle & Brevik, 2014) and additional empirical evidence. Until now, research on soil mapping with proximal sensor fusion has largely centered on locations in Australia, eastern Canada, Sweden, and the Netherlands. Applying proximal sensor fusion at sites in eastern North Dakota, United States, adds valuable empirical evidence to the expected performance of proximal sensors in different pedological settings.

Recent literature has evaluated the success of soil property predictions, but the actual value of those predictions for the agriculture industry has not been clearly communicated. Most often, models are evaluated by how much better the prediction is than the mean (R^2) and by some error metric, such as root mean square error. Instead of communicating only model validation statistics, the question of greater interest for applied research should be: "Is the prediction useful for decision making or not?" The answer depends on a combination of the model validation statistics and the threshold of soil property variability that actually affects management. For instance, it is possible for model validation statistics to be very good while the range of predicted values is too small to affect management decisions. Although determining the thresholds of soil property variability that affect management is outside the scope of this work, Chapter 2 approaches soil property prediction with these considerations in mind.

The value of soil property predictions in the agriculture industry is also closely tied to cost effectiveness. A major component of cost is the number of soil sample calibrations that are necessary for prediction. Techniques for optimizing soil sample locations and sizes with the help of covariate data are relatively recent and limited (Brus, 2019; Ramirez-Lopez et al., 2019; Van Arkel & Kaleita, 2014). Much of the research in the literature calibrated their soil property predictions with upwards of at least 30 soil samples (Castrignanò et al., 2012; Ji et al., 2019). The value of proximal sensing for the precision agriculture industry would be increased if proximal sensor fusion enables significant reduction of soil sample calibration sizes while still obtaining useful soil maps. The simple methods of soil mapping with only 15 soil samples in Chapter 2 speaks directly to this opening in precision management.

With these areas of further study in mind, Chapter 2 addresses the following objectives at three agricultural fields in eastern North Dakota, United States: 1) determine soil property predictions for bulk density, texture (percent sand, silt and clay), available water capacity, and organic matter that meet validation criteria at each site, 2) recommend which predictive geophysical data type among EMI, GRS, CRNS, and elevation is expected to produce successful multiple linear regression predictions most often, and 3) evaluate feasibility of using data fusion and multiple linear regression with small sample size for soil property prediction in precision agriculture. Chapter two is in review as:

Becker, S. M., Franz, T. E., Abimbola, O., Steele, D. D., Flores, J. P., Jia, X., Scherer, T. F., Rudnick, D. R., & Neale, C. M. U. (2022). Feasibility assessment on use of proximal geophysical sensors to support precision management. *Vadose Zone Journal*.

Chapter three reiterates the gaps identified in chapter one of 1) a systematic understanding of sensor performance in specific conditions and 2) the value of proximal soil sensing to the agriculture industry in light of chapter two findings. Future work is proposed to improve understanding of the physical processes that impact sensor response and the best use of each sensor. Additionally, chapter three presents potential methods for cost-benefit analysis and sampling optimization to address the economic value of proximal soil sensing to the agriculture industry.

References

Abdu, H., Robinson, D. A., & Jones, S. B. (2007). Comparing Bulk Soil Electrical Conductivity Determination Using the DUALEM-1S and EM38-DD Electromagnetic Induction Instruments. *Soil Science Society of America Journal*, *71*(1), 189–196. https://doi.org/10.2136/sssaj2005.0394

Adamchuk, V. I., Hummel, J. W., Morgan, M. T., & Upadhyaya, S. K. (2004a). On-the-go soil sensors for precision agriculture. *Computers and Electronics in Agriculture*, *44*(1), 71–91. https://doi.org/10.1016/j.compag.2004.03.002

Adamchuk, V. I., Hummel, J. W., Morgan, M. T., & Upadhyaya, S. K. (2004b). On-the-go soil sensors for precision agriculture. *Computers and Electronics in Agriculture*, *44*(1), 71–91. https://doi.org/10.1016/j.compag.2004.03.002

Adamchuk, V. I., Morgan, M. T., & Lowenberg-Deboer, J. M. (2004). A Model for Agro-Economic Analysis of Soil pH Mapping. *Precision Agriculture*, *5*(2), 111–129. https://doi.org/10.1023/B:PRAG.0000022357.28154.eb

Andreasen, M., Jensen, K. H., Desilets, D., Franz, T. E., Zreda, M., Bogena, H. R., & Looms, M. C. (2017). Status and Perspectives on the Cosmic-Ray Neutron Method for Soil Moisture Estimation and Other Environmental Science Applications. *Vadose Zone Journal*, *16*(8), vzj2017.04.0086. https://doi.org/10.2136/vzj2017.04.0086

Andreasen, M., Jensen, K. H., Zreda, M., Desilets, D., Bogena, H., & Looms, M. C. (2016). Modeling cosmic ray neutron field measurements: MODELING COSMIC

RAY NEUTRON FIELD MEASUREMENTS. *Water Resources Research*, *52*(8), 6451–6471. https://doi.org/10.1002/2015WR018236

Baldoncini, M., Albéri, M., Bottardi, C., Chiarelli, E., Kassandra Giulia Cristina Raptisa, Strati, V., & Mantovani, F. (2019). Biomass water content effect on soil moisture assessment via proximal gamma-ray spectroscopy. *Geoderma*, *335*, 69–77.

Baldoncini, M., Albéri, M., Chiarelli, E., Giulia Cristina Raptisa, K., Strati, V., & Mantovani, F. (2018). Investigating the potentialities of Monte Carlo simulation for assessing soil water content via proximal gamma-ray spectroscopy. *Journal of Environmental Radioactivity*, *192*, 105–116.

Bennett, J. McL., Roberton, S. D., Ghahramani, A., & McKenzie, D. C. (2021). Operationalising soil security by making soil data useful: Digital soil mapping, assessment and return-on-investment. *Soil Security*, *4*, 100010. https://doi.org/10.1016/j.soisec.2021.100010

Bottardi, C., Albéri, M., Baldoncini, M., Chiarelli, E., Montuschi, M., Raptis, K. G. C., Serafini, A., Strati, V., & Mantovani, F. (2020). Rain rate and radon daughters' activity. *Atmospheric Environment*, *238*, 117728. https://doi.org/10.1016/j.atmosenv.2020.117728

Brus, D. J. (2019). Sampling for digital soil mapping: A tutorial supported by R scripts. *Geoderma*, *338*, 464–480. https://doi.org/10.1016/j.geoderma.2018.07.036

Brus, D. J. (2021). Statistical approaches for spatial sample survey: Persistent misconceptions and new developments. *European Journal of Soil Science*, *72*(2), 686–703. https://doi.org/10.1111/ejss.12988

Caciolli, A., Baldoncini, M., Bezzon, G. P., Broggini, C., Buso, G. P., Callegari, I., Colonna, T., Fiorentini, G., Guastaldi, E., Mantovani, F., Massa, G., Menegazzo, R., Mou, L., Rossi Alvarez, C., Shyti, M., Zanon, A., & Xhixha, G. (2012). A new FSA approach for in situ γ ray spectroscopy. *Science of the Total Environment*, *414*, 639–645.

Carroll, T. R. (1981). AIRBORNE SOIL MOISTURE MEASUREMENT USING NATURAL TERRESTRIAL GAMMA RADIATION: *Soil Science*, *132*(5), 358–366. https://doi.org/10.1097/00010694-198111000-00006

Castrignanò, A., Buttafuoco, G., Quarto, R., Parisi, D., Viscarra Rossel, R. A., Terribile, F., Langella, G., & Venezia, A. (2018). A geostatistical sensor data fusion approach for delineating homogeneous management zones in Precision Agriculture. *CATENA*, *167*, 293–304. https://doi.org/10.1016/j.catena.2018.05.011

Castrignanò, A., Wong, M. T. F., Stelluti, D., De Benedetto, D., & Sollitto, D. (2012). Use of EMI, gamma-ray emission and GPS height as multi-sensor data for soil characterisation. *Geoderma*, *175–176*, 78–89. http://dx.doi.org/10.1016/j.geoderma.2012.01.013

Chatterjee, S., Hartemink, A. E., Triantafilis, J., Desai, A. R., Soldat, D., Zhu, J., Townsend, P. A., Zhang, Y., & Huang, J. (2021). Characterization of field-scale soil variation using a stepwise multi-sensor fusion approach and a cost-benefit analysis. *CATENA*, *201*, 105190. https://doi.org/10.1016/j.catena.2021.105190

de Groot, A. V., van der Graaf, E. R., de Meijer, R. J., & Maučec, M. (2009). Sensitivity of in-situ γ-ray spectra to soil density and water content. *Nuclear Instruments and Methods in Physics Research Section A: Accelerators, Spectrometers, Detectors*

and Associated Equipment, *600*(2), 519–523. https://doi.org/10.1016/j.nima.2008.12.003

Dierke, C., & Werban, U. (2013). Relationships between gamma-ray data and soil properties at an agricultural test site. *Geoderma*, *199*, 90–98. https://doi.org/10.1016/j.geoderma.2012.10.017

Doolittle, J. A., & Brevik, E. C. (2014). The use of electromagnetic induction techniques in soils studies. *Geoderma*, *223–225*, 33–45. https://doi.org/10.1016/j.geoderma.2014.01.027

Evett, S. R., O'Shaughnessy, S. A., Andrade, M. A., Kustas, W. P., Anderson, M. C., Schomberg, H. H., & Thompson, A. (2020). Precision Agriculture and Irrigation: Current U.S. Perspectives. *Transactions of the ASABE*, *63*(1), 57–67. https://doi.org/10.13031/trans.13355

Finkenbiner, C. E., Franz, T. E., Gibson, J., Heeren, D. M., & Luck, J. (2019). Integration of hydrogeophysical datasets and empirical orthogonal functions for improved irrigation water management. *Precision Agriculture*, *20*(1), 78–100. https://doi.org/10.1007/s11119-018-9582-5

Florinsky, I. V., Eilers, R. G., Manning, G. R., & Fuller, L. G. (2002). Prediction of soil properties by digital terrain modelling. *Environmental Modelling and Software*, *17*(3), 295–311. https://doi.org/10.1016/S1364-8152(01)00067-6

Franz, T. E., Zreda, M., Ferre, T. P. A., Rosolem, R., Zweck, C., Stillman, S., Zeng, X., & Shuttleworth, W. J. (2012). Measurement depth of the cosmic ray soil moisture probe affected by hydrogen from various sources: MEASUREMENT DEPTH OF THE COSMIC-RAY SOIL MOISTURE PROBE. *Water Resources Research*, *48*(8). https://doi.org/10.1029/2012WR011871

Franz, T. E., Zreda, M., Rosolem, R., Hornbuckle, B. K., Irvin, S. L., Adams, H., Kolb, T. E., Zweck, C., & Shuttleworth, W. J. (2013). Ecosystem-scale measurements of biomass water using cosmic ray neutrons: ECOSYSTEM MEASUREMENTS OF BIOMASS WATER. *Geophysical Research Letters*, *40*(15), 3929–3933. https://doi.org/10.1002/grl.50791

Gibson, J., & Franz, T. E. (2018). Spatial prediction of near surface soil water retention functions using hydrogeophysics and empirical orthogonal functions. *Journal of Hydrology*, *561*, 372–383. https://doi.org/10.1016/j.jhydrol.2018.03.046

Grasty, R. L. (1997). Radon emanation and soil moisture effects on airborne gamma-ray measurements. *Geophysics*, *62*(5), 1379–1385.

Grunwald, S., Vasques, G. M., & Rivero, R. G. (2015). Fusion of Soil and Remote Sensing Data to Model Soil Properties. In *Advances in Agronomy* (Vol. 131, pp. 1–109). Elsevier. https://doi.org/10.1016/bs.agron.2014.12.004

Heggemann, T., Welp, G., Amelung, W., Angst, G., Franz, S. O., Koszinski, S., Schmidt, K., & Pätzold, S. (2017). Proximal gamma-ray spectrometry for site-independent in situ prediction of soil texture on ten heterogeneous fields in Germany using support vector machines. *Soil and Tillage Research*, *168*, 99–109. https://doi.org/10.1016/j.still.2016.10.008

Hendriks, P. H. G. M., Limburg, J., & de Meijer, R. J. (2001). Full-spectrum analysis of natural γ-ray spectra. *Journal of Environmental Radioactivity*, *53*(3), 365–380. https://doi.org/10.1016/S0265-931X(00)00142-9

IAEA. (2003). *Guidelines for radio element mapping using gamma ray spectrometry data* (No. 1363; Technical Documents). International Atomic Energy Agency.

Ji, W., Adamchuk, V. I., Chen, S., Biswas, A., Mat Su, A. S., Ismail, A., Gan, Q., & Shi, Z. (2019). Simultaneous measurement of multiple soil properties through proximal sensor data fusion: A case study. *Geoderma*, *341*, 111–128.

Jiménez-Jiménez, S. I., Ojeda-Bustamante, W., Marcial-Pablo, M., & Enciso, J. (2021). Digital Terrain Models Generated with Low-Cost UAV Photogrammetry: Methodology and Accuracy. *ISPRS International Journal of Geo-Information*, *10*(5), 285. https://doi.org/10.3390/ijgi10050285

Köhli, M., Schrön, M., Zreda, M., Schmidt, U., Dietrich, P., & Zacharias, S. (2015). Footprint Characteristics Revised for Field-Scale Soil Moisture Monitoring with Cosmic-Ray Neutrons. *Water Resources Research*, *51*(7), 5772–5790. https://doi.org/10.1002/2015WR017169

Lo, T., Heeren, D. M., Martin, D. L., Mateos, L., Luck, J. D., & Eisenhauer, D. E. (2016). Pumpage Reduction by Using Variable-Rate Irrigation to Mine Undepleted Soil Water. *Transactions of the ASABE*, *59*(5), 1285–1298. https://doi.org/10.13031/trans.59.11773

Lowenberg-DeBoer, B. E. | J. (2017, June 1). 2017 Precision Dealership Survey: Making the Turn Toward Decision Agriculture. *CropLife*. https://www.croplife.com/iron/2017-precision-dealership-survey-making-the-turn-toward-decision-agriculture/

Mahmood, H. S. M., Hoogmoed, W. B., & van Henten, E. J. (2013). Proximal Gamma-Ray Spectroscopy to Predict Soil Properties Using Windows and Full-Spectrum Analysis Methods. *Sensors*, *13*, 16263–16280. https://doi.org/10.3390/s131216263

Malone, B. P., de Gruijter, J. J., McBratney, A. B., Minasny, B., & Brus, D. J. (2011). Using Additional Criteria for Measuring the Quality of Predictions and Their Uncertainties in a Digital Soil Mapping Framework. *Soil Science Society of America Journal*, *75*(3), 1032–1043. https://doi.org/10.2136/sssaj2010.0280

McBratney, A. B., Minasny, B., & Whelan, B. M. (2005). Obtaining 'useful' high-resolution soil data from proximally-sensed electrical conductivity/resistivity (PSEC/R) Surveys. In J. V. Stafford (Ed.), *Precision Agriculture '05: Proceedings of the 5th European Conference on Precision Agriculture*. Wageningen Academic Publishers. https://doi.org/10.3920/978-90-8686-549-9

McBratney, A., Minasny, B., & Whelan, B. M. (2005). Obtaining 'useful' high-resolution soil data from proximally-sensed electrical conductivity/resistivity (PSEC/R) surveys. In J. V. Stafford (Ed.), *Precision Agriculture '05* (pp. 503–510). Wageningen Academic Publishers.

Megumi, K., & Mamuro, T. (1977). Concentration of uranium series nuclides in soil particles in relation to their size. *Journal of Geophysical Research*, *82*(2), 353–356. https://doi.org/10.1029/JB082i002p00353

Morris, E. R. (2009). Height-above-ground effects on penetration depth and response of electromagnetic induction soil conductivity meters. *Computers and Electronics in Agriculture*, *68*(2), 150–156. https://doi.org/10.1016/j.compag.2009.05.009

Polidori, L., & El Hage, M. (2020). Digital Elevation Model Quality Assessment Methods: A Critical Review. *Remote Sensing*, *12*(21), 3522. https://doi.org/10.3390/rs12213522

Priori, S., Bianconi, N., & Costantini, E. A. C. (2014). Can γ-radiometrics predict soil textural data and stoniness in different parent materials? A comparison of two machine-learning methods. *Geoderma*, *226–227*, 354–364. https://doi.org/10.1016/j.geoderma.2014.03.012

Ramirez-Lopez, L., Wadoux, A. M. J. -C., Franceschini, M. H. D., Terra, F. S., Marques, K. P. P., Sayão, V. M., & Demattê, J. A. M. (2019). Robust soil mapping at the farm scale with vis–NIR spectroscopy. *European Journal of Soil Science*, *70*(2), 378–393. https://doi.org/10.1111/ejss.12752

Rodrigues Jr., F. A., Bramley, R. G. V., & Gobbett, D. L. (2015). Proximal soil sensing for Precision Agriculture: Simultaneous use of electromagnetic induction and gamma radiometrics in contrasting soils. *Geoderma*, *243–244*, 183–195. http://dx.doi.org/10.1016/j.geoderma.2015.01.004

Rossel, R. A. V., Taylor, H. J., & McBratney, A. B. (2007). Multivariate calibration of hyperspectral γ-ray energy spectra for proximal soil sensing. *European Journal of Soil Science*, *58*(1), 343–353. https://doi.org/10.1111/j.1365-2389.2006.00859.x

Schimmelpfennig, D. (Ed.). (2016). *Farm Profits and Adoption of Precision Agriculture*. https://doi.org/10.22004/ag.econ.249773

Söderstrom, M., Sohlenius, G., Rodhe, L., & Piikki, K. (2016). Adaptation of regional digital soil mapping for precision agriculture. *Precision Agriculture*, *17*, 588–607.

Taylor, J. A., Short, M., McBratney, A. B., & Wilson, J. (2010). Comparing the Ability of Multiple Soil Sensors to Predict Soil Properties in a Scottish Potato Production System. In R. A. Viscarra Rossel, A. B. McBratney, & B. Minasny (Eds.), *Proximal Soil Sensing* (pp. 387–396). Springer Netherlands. https://doi.org/10.1007/978-90-481-8859-8_33

Triantafilis, J., & Lesch, S. M. (2005). Mapping clay content variation using electromagnetic induction techniques. *Computers and Electronics in Agriculture*, *46*(1–3), 203–237. https://doi.org/10.1016/j.compag.2004.11.006

Van Arkel, Z., & Kaleita, A. L. (2014). Identifying sampling locations for field-scale soil moisture estimation using K-means clustering. *Water Resources Research*, *50*(8), 7050–7057. https://doi.org/10.1002/2013WR015015

van der Klooster, E., van Egmond, F. M., & Sonneveld, M. P. W. (2011). Mapping soil clay contents in Dutch marine districtsusing gamma-ray spectrometry. *European Journal of Soil Science*, *62*(5), 743–753.

van der Veeke, S., Limburg, J., Koomans, R. L., Söderström, M., de Waal, S. N., & van der Graaf, E. R. (2021). Footprint and height corrections for UAV-borne gamma-ray spectrometry studies. *Journal of Environmental Radioactivity*, *231*. https://doi.org/10.1016/j.jenvrad.2021.106545

van Egmond, F. M., Loonstra, E. H., & Limburg, J. (2010). *Gamma-ray sensor for topsoil mapping; the Mole* (p. 10). The Medusa Institute. https://the.medusa.institute/display/GW/Publications

Viscarra Rossel, R. A., Cattle, S. R., Ortega, A., & Fouad, Y. (2009). In situ measurements of soil colour, mineral composition and clay content by vis–NIR

spectroscopy. *Geoderma*, *150*(3–4), 253–266. https://doi.org/10.1016/j.geoderma.2009.01.025

Visconti, F., & De Paz, J. M. (2021). A semi-empirical model to predict the EM38 electromagnetic induction measurements of soils from basic ground properties. *European Journal of Soil Science*, *72*(2), 720–738. https://doi.org/10.1111/ejss.13044

Wong, M. T. F., & Harper, R. J. (1999). Use of on-ground gamma-ray spectrometry to measure plant-available potassium and other topsoil attributes. *Soil Research*, *37*(2), 267. https://doi.org/10.1071/S98038

Wong, M. T. F., Oliver, Y. M., & Robertson, M. J. (2009). Gamma-Radiometric Assessment of Soil Depth across a Landscape Not Measurable Using Electromagnetic Surveys. *Soil Science Society of America Journal*, *73*(4), 1261–1267. https://doi.org/10.2136/sssaj2007.0429

Zhang, Y., Ji, W., Saurette, D. D., Easher, T. H., Li, H., Shi, Z., Adamchuk, V. I., & Biswas, A. (2020). Three-dimensional digital soil mapping of multiple soil properties at a field-scale using regression kriging. *Geoderma*, *366*, 114253. https://doi.org/10.1016/j.geoderma.2020.114253

Zhu, Y., Weindorf, D. C., & Zhang, W. (2011). Characterizing soils using a portable X-ray fluorescence spectrometer: 1. Soil texture. *Geoderma*, *167–168*, 167–177. https://doi.org/10.1016/j.geoderma.2011.08.010

Zreda, M., Desilets, D., Ferré, T. P. A., & Scott, R. L. (2008). Measuring soil moisture content non-invasively at intermediate spatial scale using cosmic-ray neutrons. *Geophysical Research Letters*, *35*(21), L21402. https://doi.org/10.1029/2008GL035655

Zreda, M., Shuttleworth, W. J., Zeng, X., Zweck, C., Desilets, D., Franz, T., & Rosolem, R. (2012). COSMOS: The COsmic-ray Soil Moisture Observing System. *Hydrology and Earth System Sciences*, *16*(11), 4079–4099. https://doi.org/10.5194/hess-16-4079-2012

CHAPTER 2

FEASIBILITY ASSESSMENT ON USE OF PROXIMAL GEOPHYSICAL SENSORS TO SUPPORT PRECISION MANAGEMENT

Sophia M. Becker[1], Trenton E. Franz[1], Olufemi Abimbola[1], Dean D. Steele[2], J. Paulo Flores[2], Xinhua Jia[2], Thomas F. Scherer[2], Daran R. Rudnick[3], Christopher M. U. Neale[4]

[1]School of Natural Resources, University of Nebraska–Lincoln, Lincoln, Nebraska, USA

[2]Agricultural and Biosystems Engineering Department, North Dakota State University, Fargo, North Dakota, USA

[3]West Central Research and Extension Center, University of Nebraska-Lincoln, and Robert B. Daugherty Water for Food Global Institute at the University of Nebraska Faculty Fellow, North Platte, NE, USA

[4]Robert B. Daugherty Water for Food Global Institute at the University of Nebraska, Biological Systems Engineering Department, University of Nebraska-Lincoln, Lincoln, NE, USA

2.1 Introduction

Predictive soil mapping with proximal geophysical data has potential to benefit precision agriculture because proximal sensors such as the gamma-ray sensor (GRS; IAEA, 2003; van der Veeke et al., 2021), cosmic-ray neutron sensors (CRNS; Zreda et al., 2008; Desilets et al., 2010), and electromagnetic induction (EMI; Abdu, 2008; Gibson and Franz, 2018) have footprint sizes that can characterize soil on the subfield scale. In the United States, field sizes vary widely depending on region and crop

type, but the median field size is 27.8 hectares (Yan and Roy, 2016), and management on the subfield scale (around 0.4 hectare) is possible because of recent advancements in fertilizer, planter, sprayer, and irrigation equipment (Hamrita et al., 2000; O'Shaughnessy et al., 2019). Precision agriculture manages inputs such as water, fertilizer, and seeding rate and variety on a subfield scale to maximize profit, which often means maximizing yield while optimizing the timing and placement of input resources. Soil texture, pH, available water capacity, cation exchange capacity, electrical conductivity, and organic matter content are all related to setting and obtaining yield goals and considered valuable information for precision management decisions (Shearer and Ward, 1999). Possible variable management responses to soil maps that portray subfield variation include irrigation, seeding rate, tillage settings, liming, and application of compost and fertilizer (van Egmond et al., 2010). This paper aims to determine if predictive soil maps useful for variable management can be created with a combination of proximal geophysical data sources and in-field soil sampling.

Data fusion, or using multiple data sources as predictive data, is a common approach for predicting soil properties. Combinations explored in the past have included EMI, GRS, elevation, and visible and near-infrared data. Rodrigues Jr. et al. (2015) used EMI and GRS and found that, using principal components, regression models of clay and cation exchange capacity were significant ($p < .05$) at five out of eight study sites. Castrignanò et al. (2012) found that different soils in Western Australia that produced similar responses in a single sensor (sandy, sandy gravelly, sandy salt-affected, and clayey soils) could be discriminated when using combined EMI, GRS, and elevation. Additionally, Castrignanò et al. found correlation ($r \geq .46$) between GRS and soil organic

carbon (SOC), plant-available potassium (K), and phosphorous (P), and found weaker correlation ($r \leq .31$) between EMI and P and pH. Elevation was correlated with SOC, plant-available K, and P with correlation coefficients of .28 to .39. In another study, Ji et al. (2019) could not predict extractable K and P with combined information from elevation, GRS, EMI, and visible and near-infrared data. However partial least-squares regressions of soil organic matter, pH, lime buffering capacity, calcium, magnesium, and aluminum were usually improved by substituting the data fusion approach for a single sensor, obtaining $R^2 > .5$.

The present study combines EMI, GRS, CRNS, and elevation data. Each of these measurements is theoretically related to a variety of soil characteristics. EMI measures apparent bulk electrical conductivity, which is affected by soil water content, soil temperature, clay content, mineralogy, bulk density, and salinity (McBratney et al., 2005; Franz et al., 2017). Gamma-ray sensors detect naturally emitted gamma radiation from K-40 and the gamma-rays emitted by the U-238 and Th-232 decay series. Detected gamma radiation is influenced by soil water content, parent material mineralogy, organic matter, and texture (Carroll, 1981; Dierke and Werban, 2013). CRNS measures low-energy neutron counts (~0.25 – 1000 eV), which are an established method for soil water estimation (Zreda et al., 2008). Low-energy neutron counts may also serve as a proxy for overall soil variability related to properties such as organic matter content or available water capacity (Andreasen et al., 2017; Finkenbiner et al., 2019). Elevation is connected to soil formation, soil water, and organic carbon content (Florinsky et al., 2002). The predictive data suite comprised of EMI, GRS, CRNS, and elevation data allows this study

to freshly examine any possible correlations between these proximal sensing data and soil properties of interest.

Soil mapping with data fusion is intriguing not only because of the wide range of potential data combinations, but also because the relative performances of different predictive data types vary across settings. Wong and Harper (1999) concluded that the usefulness of gamma-ray spectroscopy alone is limited because relationships between K-40 counts and soil properties did not hold everywhere for sites in Western Australia. This suggests that site specific calibrations are required for soil property predictions with gamma-ray data and that inclusion of additional sensors would be informative. For instance, in Queensland and South Australia, Rodrigues Jr. et al. (2015) found that predictions of clay and cation exchange capacity were improved by using principal components from EMI and gamma-ray data as predictors versus predicting with EMI or gamma-ray data alone. However, the geophysical information most strongly correlated with a given soil property differed between field sites of varying pedology and geographic location. Rodrigues Jr. et al. also explored universal calibration for Australian soils by combining sensor and soil sample data from all their sites and found adjusted R^2 values of .27 and .22 for predictions of CEC and clay, respectively. The varying results of data fusion in different settings mean that each analysis of a new site adds valuable information to our understanding of which geophysical sensor is most crucial in given situations. Because the GRS, CRNS, and EMI explore different wavelengths on the electromagnetic spectrum, we expect each sensor to obtain novel information. Similar to use of visible and near-infrared bands to calculate the normalized difference vegetation

index (NDVI), this paper pursues integration of GRS, CRNS, EMI, and elevation into new information that characterizes the field.

Understanding the proper situations for different sensors will inform producers and researchers as they navigate the numerous commercial soil mapping technologies available. At least one soil mapping company, SoilOptix (Canada), has arisen that provides gamma-ray mapping technology and support, suing sensors produced by Medusa Radiometrics (Netherlands). EMI and direct current resistivity are standard soil mapping capabilities offered by numerous companies. CRNS is still an emerging technology, but the sensor is commercially available through several companies such as Hydroinnova, LLC (Albuquerque, NM). Given the current accessibility of commercial EMI, GRS and CRNS surveys, determining the predictive ability of these tools in new agricultural contexts is extremely timely.

Predictive soil mapping methods in the literature include support vector machine, random forest, classification and regression trees, partial least squares regression (PLSR), bagging-PLSR, multivariate adaptive regression splines, K nearest neighbor, and co-kriging (Ji et al., 2019; Rossel et al., 2007; Söderstrom et al., 2016; Piikki et al., 2013; Castrignanò et al., 2012). In addition to the more complex modeling approaches, multiple linear regression (MLR) also has extensive precedent due to its simplicity (Mahmood et al., 2013; van Egmond et al., 2010; van der Klooster et al., 2011) and high interpretability. In our analysis we utilize MLR since it is pragmatic given the expected and desired small soil sample sizes usually attainable by producers and crop consultants.

The cost and time required for soil core sampling limits methods in both precision agriculture and other aspects of the agriculture industry. Another sector needing maximal

information return on few soil samples is the monitoring, verification, and reporting of SOC. The SOC market has the potential to be a viable source of income for producers, but the system is limited by poor information on producers' actual SOC storage. Third party companies verify the carbon credits that farmers sell, and this verification service comprises roughly 75% of the total cost of producing carbon credits (Plume, 2021). This study addresses how well SOC (or organic matter here) can be predicted from limited samples with the help of geophysical surveys, and which geophysical data types are preferred.

The hypothesis of this study is that EMI, GRS, CRNS, and elevation data layers are all useful in multiple linear regression predictions of soil properties that meet expert criteria at three agricultural sites in North Dakota, United States. The objectives are to: 1) determine soil property predictions for bulk density, texture (percent sand, silt and clay), available water capacity, and organic matter that meet validation criteria at each site, 2) recommend which predictive geophysical data type among EMI, GRS, CRNS, and elevation is expected to produce successful multiple linear regression predictions most often, and 3) evaluate feasibility of using data fusion and multiple linear regression with small sample size for soil property prediction in precision agriculture.

2.2 Methodology

2.2.1 Study Sites

Each of the three sites considered in this study is a roughly 53 ha agricultural field located in southeast North Dakota, United States. The sites were selected based on the following criteria: 1) they had an existing or prior USDA-NRCS Environmental Quality

Incentives Program contract on variable rate irrigation, 2) the water table was below the crop rooting zone, and 3) the sites were relatively close to Fargo, North Dakota. Average annual rainfall for the region during the time period 2007 – 2020 is 448 mm and annual potential evapotranspiration is 1262 mm (North Dakota Agricultural Weather Network, 2021; Lisbon station). For southeastern North Dakota, the normal monthly low temperature ranges from -17.9 ℃ (January) to 14.7 ℃ (July), and the normal monthly high temperature ranges from -7.5 ℃ (January) to 27.8 ℃ (July). Normal temperatures reported here are from the period 1991 – 2020 as reported by the National Weather Service. All fields are center pivot irrigated. The crops grown at sites 1, 2, and 3 in 2020 were soybeans [*Glycine max* (L.) Merr.], potatoes (*Solanum tuberosum* L.), and maize (*Zea mays* L.), respectively, with growing seasons from May through September. Southeastern North Dakota generally experiences its first killing frost around October 1 and the soil is free of frost again around April 1. At site 1, wetlands fill depressions on the east (7.5 ha) and south (6.7 ha) sides of the field. Site 2 has a moraine feature in the southeast corner of the field with a maximum height of 11 m above the rest of the field. A shallow depression is oriented west-northwest through the middle of site 3.

In southeast North Dakota, the surface geology is a patchwork of till, glacial outwash, deltaic deposits, glacial lacustrine sediment, and aeolian sand (Bluemle, 1975). Locations of the field sites amidst the variable surface geology are shown in Figure 2.1.

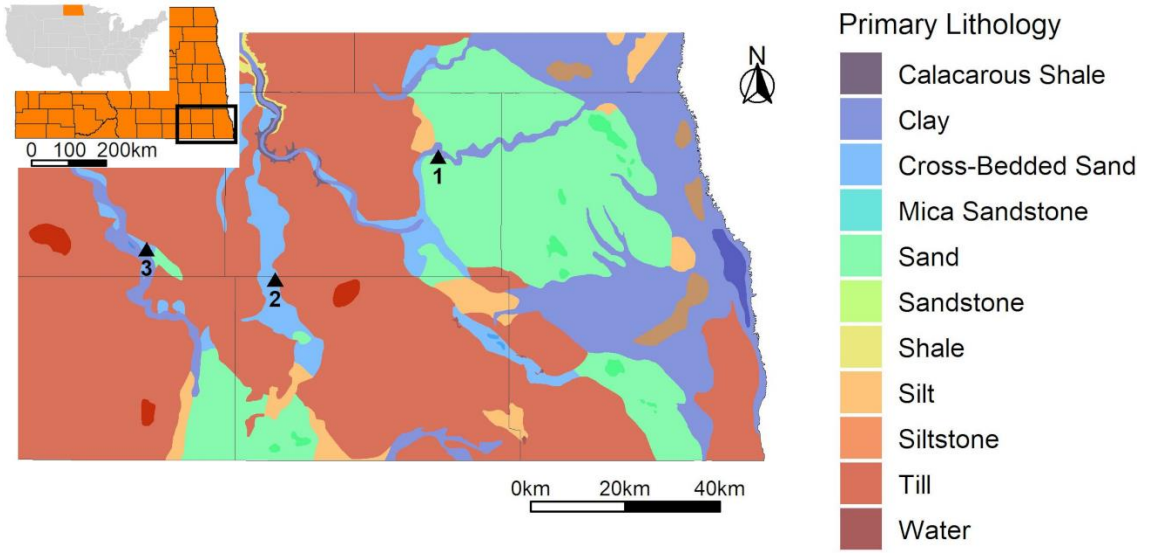

Figure 2.1. Surficial geology of southeast North Dakota, United States (units grouped by primary lithology type). Locations of sites 1, 2 and 3 are plotted with black triangles.

Site 1 lies on a Holocene aeolian sand deposit about one km south of the Sheyenne River. Site 2 is on a Holocene glacial outwash deposit of cross-bedded sand and plane-bedded gravel. Site 3 also sits on a Holocene deposit of bedded sand and gravel, about a half km northeast of the modern James River (State of North Dakota, NDGISHUB Surface Geology). The unconsolidated sediments at all three sites are underlain by Cretaceous calcareous shale: the Greenhorn Formation at site 1 and the Niobrara Formation at sites 2 and 3 (State of North Dakota, NDGISHUB Bedrock Geology). Generally, the soil types at all the sites are loams or sandy loams. Figure 2.2 depicts the soil series present in each field in greater detail.

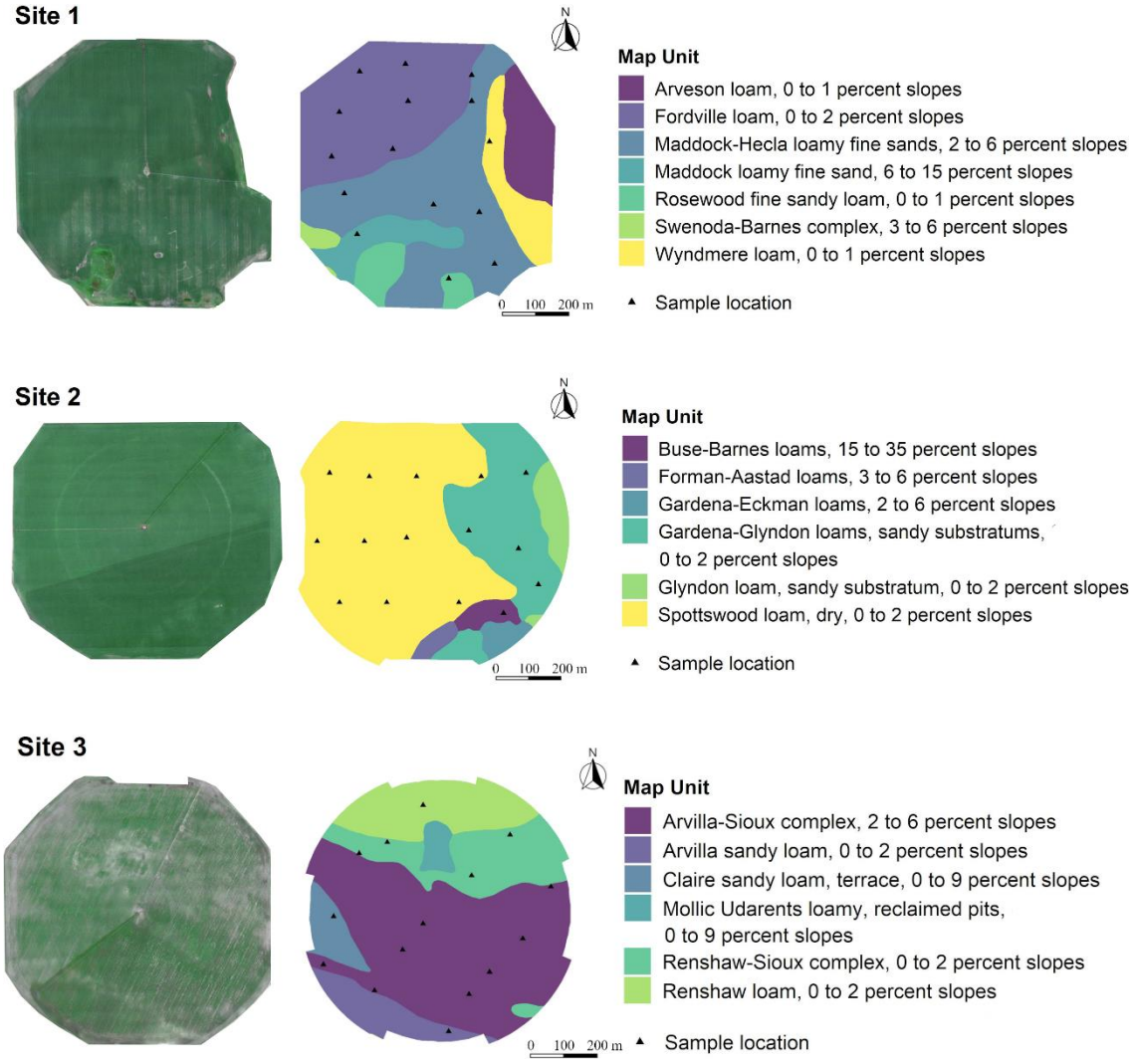

Figure 2.2. Drone-surveyed RGB images, soil types, and sample locations at site 1, 2, and 3.

2.2.2 Geophysical data collection and processing

Geophysical surveys were performed on 15 October 2020 at sites 1 and 2 and on 16 October 2020 at site 3. EMI, CRNS, and GRS data were simultaneously collected from a vehicle traveling approximately 10-15 km h^{-1} in transects spaced roughly 10 m apart.

EMI was performed with a DUALEM-21 sensor, pulled in a plastic sled behind the vehicle, to obtain apparent bulk electrical conductivity data in mS m^{-1}. Shallow apparent bulk electrical conductivity (ECaS), deep apparent bulk electrical conductivity (ECaD), and ratio of shallow to deep electrical conductivity (ECaSDR) were recorded. Only the 2 m coil spacing array was used. The horizontal co-planar coil orientation penetrates the surface to about 1 m depth (ECaS), and the perpendicular coil orientation penetrates to roughly 2.5 – 3 m depth (ECaD; Dualem Inc., 2013). Soundings were recorded every second, and the location of each measurement was recorded with a Hemisphere GPS XF101 DGPS (Juniper Systems, Inc., Logan, UT) unit Outliers and redundant data were removed from the raw ECa data to assure basic quality.

A passive, vehicle-mounted cosmic-ray neutron detector (eight ~1.8m CRS 2000/B tube capsules from Hydroinnova, LLC, Albuquerque, NM) recorded accumulated neutron counts in 1-minute intervals (units of counts per minute, cpm). The measurement volume was a disk with diameter ~400 m and depth ranging from 0.12 to 0.76 m (Zreda et al., 2008; Köhli, 2015). Neutron moderation power of the soil is controlled by hydrogen, so the flux of epithermal or fast neutrons detected at the soil surface is inversely proportional to soil water content (Zreda et al., 2012; Desilets et al., 2010). From the neutron counts, volumetric soil water content (SWC) was estimated in cm^3/cm^3 with a nonlinear calibration function following Franz et al. (2015).

Gamma-ray spectra were collected with a 2.5 L NaI(Tl) scintillation crystal with 512 channels, made by Hydroinnova (Albuquerque, New Mexico). The detector was mounted on the vehicle and collection time for each spectrum was 10 s. Detector position was recorded via GPS at the beginning of each 10 s measurement period. The midpoint

between the detector location at beginning of the measurement period and end of the measurement period was used as the location for the corresponding gamma-ray spectrum. Gamma-rays that are detected by the spectrometer are emitted from the top 30-60 cm of the soil. The stationary 65% footprint of the gamma-ray spectrometer, when mounted at 1.5 m height, is described by a circle that has a radius of 3.8 m. 65% of the radiation detected by the gamma-ray spectrometer is emitted by a volume that lies within this circle. The 95% footprint has a radius of 24 m, and therefore it can be advised for the interpretation that the static spectrometer collects gamma-ray from an area that has a radius < 24 m (van der Veeke et al., 2021). Using a generic calibration based on detector specifications, Gamman software (Medusa Radiometrics, Groningen, Netherlands) was used to analyze gamma-ray spectra and determine activity concentrations of K-40, U-238, and Th-232. Gamman performs energy stabilization and then uses the non-negative least squares full-spectrum analysis (NNLS-FSA) approach to find radioelement concentrations (Hendriks, 2001; Caciolli et al., 2012).

A digital surface model (DSM) from each field, after harvest, was created from images collected with a DJI Phantom 4 RTK (DJI – Shenzhen, China) unmanned aircraft system (UAS). The aircraft is equipped with a 20-megapixel RGB camera (5472 x 3648 pixels), and it was flown at 61 m (200 ft) above ground level, with front and side overlap of 75%. To assure high spatial accuracy, the UAS was connected during the flights to an internet based virtual base network (VBN) provided by DigiFarm (Monticello, IA), which resulted in images geotagged with real time kinematics precision (0.02 m accuracy). For redundancy, we used eight ground control points (GCPs) spread across each field. Five-gallon pail lids (area of 0.07 m^2) were used for that purpose, and a

Trimble Geo7x GPS unit (Trimble - Sunnyvale, CA), connected to the same VBN mentioned above, was used to survey the center of each GCP (0.02 m accuracy). The images were stored in SD card during flights, and later they were transfer to desktop computer to be processed. The images were first processed (stitched) with Pix4Dmapper from Pix4D (Pix4D SA - Lausanne, Switzerland), resulting in a DSM with average ground sample distance across sites of 0.018 cm/pixel. Since the field level analysis did not require such high resolution as of the DSMs generated from the stitching process, ArcGIS Pro (ESRI – West Redlands, CA) software was used to resample those to a 1 m/pixel resolution prior to further analysis.

All covariate data measurements were translated to a 10 by 10 m grid, where the value of each grid node was the average of all surrounding data points within a specified radius. A 70m radius was used for all data types except for gamma-ray data at Site 1, where the radius was decreased to 31m to avoid an artificial spatial pattern that arose when a search radius of 70m was used. Geophysical data smoothed to the 10 by 10 m grid was then interpolated in Surfer mapping software (Golden Software LLC, Golden, CO) with ordinary kriging to full field extent and grid cell size of 2 m to create a complete covariate table for model prediction. The spatial continuity and stationarity assumptions of kriging are believed to be reasonable in this field soil mapping scenario. Multiple variogram models (linear, spherical, Gaussian, exponential) were constructed for each geophysical data type, and the resulting interpolation with lowest median absolute deviation of residuals (from 100 randomly selected points) was chosen for model training and prediction.

2.2.3 Soil Sampling and Laboratory Analyses

Sites 1, 2, and 3 were sampled on 20, 21, and 26 October 2020, respectively. Typical soil sampling is done every hectare, but cost and labor required for hydraulic property analysis limited this study to 15 samples per 53 ha. Moreover, in most agricultural applications, the number of soil samples will be limited to 1 sample per ha or even fewer following university extension guidelines. Optimal placement of such limited soil samples has been discussed elsewhere; see Lesch et al. (2000) for USDA soil salinity sampling based on EMI and see Gibson and Franz (2018) for soil hydraulic property sampling based on EMI and CRNS. Here, sampling locations were primarily selected based on uniform spacing. Slight position modifications were made to capture soil types based on visual examination of ECaD data, SSURGO soil zones, and elevation data. Samples were also a minimum distance of 50 m from one another. Locations of the 15 soil samples collected at each site are given in Figure 2. Two cores were collected at each location using a 57-mm outside diameter (54 mm inside diameter of bit) × 1.2-m long, slotted soil sampling tube (Model ST-108, Giddings Machine Company, Inc., Windsor, Colorado). The sampling tube was driven into the soil by a hydraulic soil sampling machine (#15-SCS/Model GSRPS or similar, Giddings). The soil cores were aggregated by depth intervals of 0 – 0.30 m, 0.30 - 0.61 m, and 0.61 - 0.91 m.

Eight soil properties were estimated in the laboratory: cation exchange capacity (CEC), pH, electrical conductivity (EC), organic matter, bulk density, texture (percent sand, silt, and clay), field capacity (FC), and permanent wilting point (PWP). Available water capacity (AWC) was determined as FC – PWP, for a total of nine soil properties. Only relatively static soil properties were considered in this analysis. Cation exchange

capacity, pH, EC, and organic matter were determined by the Soil Testing Lab (STL) at North Dakota State University, Fargo, North Dakota. Organic matter content was measured by weight loss on ignition (Combs & Nathan, 2015). Bulk density was determined in the laboratory based on oven drying of field samples. Texture was determined with hydrometer mechanical analyses. Field capacity and PWP on a gravimetric bases were estimated with 1/3 bar and 15 bar water contents, respectively, from pressure plate analyses of 100 g of sample. Volumetric water content values of FC and PWP were determined as the product of ρ_b and gravimetric water content assuming a density of 1.0 g cm^{-3} for water, and adjustment for stones was made following Gardner (1986). In 14 cases where soil sampling depth was limited by gravel (particularly at depths below 0.30 m at Site 3), missing data were populated with values from NRCS Soil Survey Geographic database (Soil Survey Staff). The SSURGO "CEC-7" values were considered equivalent to the NDSU STL's CEC values (L. Cihacek, incoming interim STL director, 2021 personal communication).

2.2.4 Soil Property Statistical Models

Simple statistical models of the soil properties measured in the lab were built using all geophysical data types as possible predictor variables. Each sampling depth interval was modeled separately. The training set was constructed by extracting all geophysical data at the grid node closest to each of the sample locations and joining it to the sampled soil property data. Modeling was limited to multiple linear regression using ordinary least squares because only 15 soil samples were collected for calibration at each site. All modeling and prediction was carried out using the caret package in R (Version 4.0.2).

The following components of multiple linear regression were addressed: normality of error, multicollinearity, and homoscedasticity. A log base 10 transformation was applied to all predictive data to improve normality. Because we are interested in the significance of individual predictors, multicollinearity was handled by calculating the variance inflation factor (VIF) of the model and iteratively removing the variable with the highest VIF until all VIF scores of the remaining variables were less than 5. The VIF is given by

$$VIF_i = (1 - R_i^2)^{-1} \quad (1)$$

where R_i^2 is the coefficient of determination of the *i*th predictor variable regressed against all other variables. Model residuals were plotted against fitted values to evaluate homoscedasticity (see supplemental R code). To avoid overfitting, only models with 3 parameters (2 predictors and an intercept) or fewer were evaluated.

Multiple linear regression was performed on all possible 2 and 3-parameter combinations using the entire training set. The set of regression models for each soil property made up of all 2-parameter models and the 3-parameter models with the 10 highest coefficient of determination (R^2) statistics was further evaluated with leave-one-out cross-validation (LOOCV) using the "caret" package in R. P-values of the final model parameters given by LOOCV describe the significance of each predictor.

2.2.6 Map Predictions of Soil Properties

For all predicted soil properties and depth intervals, the model with lowest root mean square error of prediction (RMSEP; eq. 2) was chosen and model predictions were calculated using the covariate table of interpolated geophysical data. Predicted values were truncated according to physical constraints, which were set as the minimum lower

and maximum upper expected value within the field area according to the SSURGO data base (Table 1).

Table 2.1. Physical constraints and reasonable uncertainty limits imposed on model predictions. Constraints are given for organic matter (OM), sand, silt, clay, cation exchange capacity (CEC), electrical conductivity (EC), pH, bulk density (BD), and available water capacity (AWC).

Soil property	Site	Min	Max	Uncertainty
OM (%)	1	0	7	± 2
	2	0	8	± 2
	3	0	5.1	± 2
Sand (%)	1	25	97	± 5
	2	10	96	± 5
	3	35	97	± 5
Silt (%)	1	0	60	± 5
	2	2	75	± 5
	3	1	38	± 5
Clay (%)	1	2	35	± 5
	2	1	35	± 5
	3	0	35	± 5
CEC (meq $100g^{-1}$)	1	1.6	89	± 2
	2	1	94.7	± 2
	3	0	72.9	± 2
EC (mmhos cm^{-1})	1	0	4	± 0.1
	2	0	8	± 0.1
	3	0	3	± 0.1
pH	1	5.2	8.4	± 0.5
	2	6.1	8.4	± 0.5
	3	6.3	8.4	± 0.5
BD (g cm^{-3})	1	1.1	1.83	± 0.15
	2	1.1	1.77	± 0.15
	3	1.25	1.92	± 0.15
AWC (cm^3 cm^{-3})	1	0.02	0.21	± 0.03
	2	0.04	0.23	± 0.03
	3	0.04	0.21	± 0.03

If observed values were more extreme than those expected by the SSURGO data base, the minimum and maximum expected values were substituted as constraints. Predictions were then summarized with the following measures: RMSEP, R-squared of prediction

(R^2_{pred}), minimum, maximum, standard deviation, and mean. RMSEP and R^2_{pred} are given by

$$RMSEP = \sqrt{\frac{\sum_i^N (\hat{y}_i - y_i)^2}{N}}, \quad (2)$$

$$R^2_{pred} = \frac{\sum_i^N (\hat{y}_i - \bar{y})^2}{\sum_i^N (y_i - \bar{y})^2}, \quad (3)$$

where $\hat{y}_i$ is the *i*th predicted value from the final model built by LOOCV, y_i is the *i*th observed value, *N* is the sample size and $\bar{y}$ is the sample mean. The RMSEP given by LOOCV was considered a reasonable estimate of the overall uncertainty in the models and was compared to generic uncertainty levels considered useful in agricultural management. Proposed uncertainty thresholds are defined in Table 2.1 based on the authors' expert knowledge.

2.3 Results

2.3.1 Geophysical data

Maps of kriged geophysical data are given in Figure 2.3. Mean and uncertainty of apparent bulk electrical conductivity, radionuclide concentrations, elevation, and neutron counts are given in Table 2.2. Among all the sites, site 3 has the smallest range in apparent bulk electrical conductivity and elevation. Elevation and ECaD were moderately correlated at site 1 and site 2, and elevation and all EMI variables were strongly correlated at site 3. ECaS and ECaD were negatively correlated with cosmic-ray neutron counts with correlation coefficients of r = - .7 and r = - .53 at site 1, and correlation coefficients of r = - .4 and r = - .39 at site 2. At site 2, elevation and cosmic-ray neutron counts were correlated with a coefficient of r = .55. K-40 was correlated with U-238 (r =

.33) and Th-232 (r = .40) at site 1, and negligibly correlated with the other radioelements at sites 2 and 3 (|r |< .26). Th-232 and U-238 were positively correlated at site 1 (r = .41), negatively correlated at site 2 (r = - .41), and negligibly correlated at site 3.

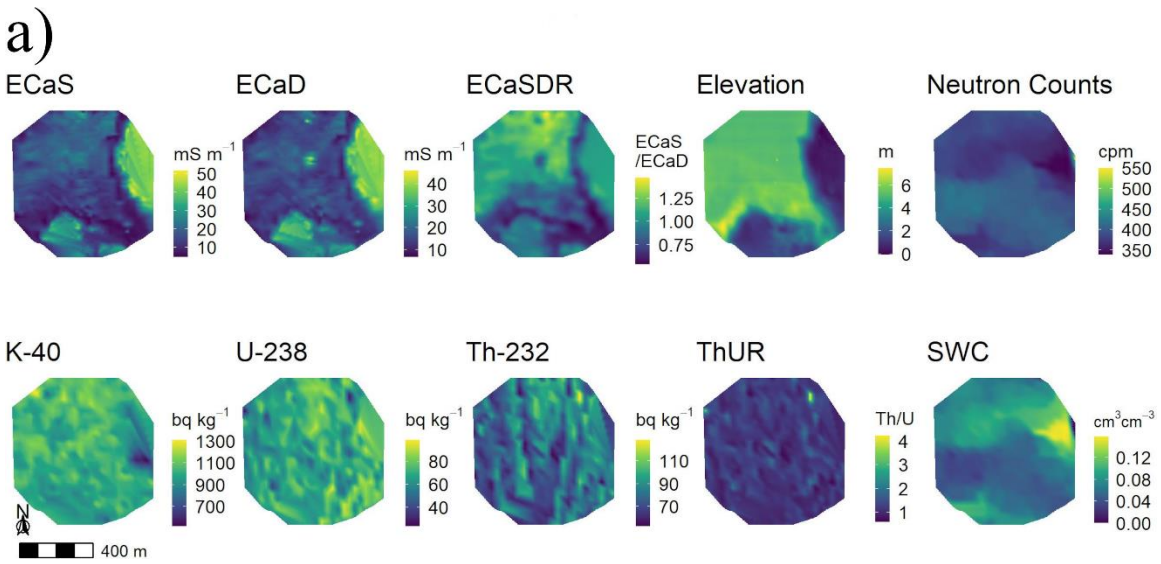

Figure 2.3a. Maps of geophysical data estimated by kriging at site 1. Shown are shallow apparent bulk electrical conductivity (ECaS), deep apparent bulk electrical conductivity (ECaD), ratio of shallow to deep apparent bulk electrical conductivity (ECaSDR), relative elevation, neutron counts, potassium (K-40), uranium (U-238), thorium (Th-232), ratio of thorium to uranium (ThUR), and soil water content estimated from neutron counts (SWC).

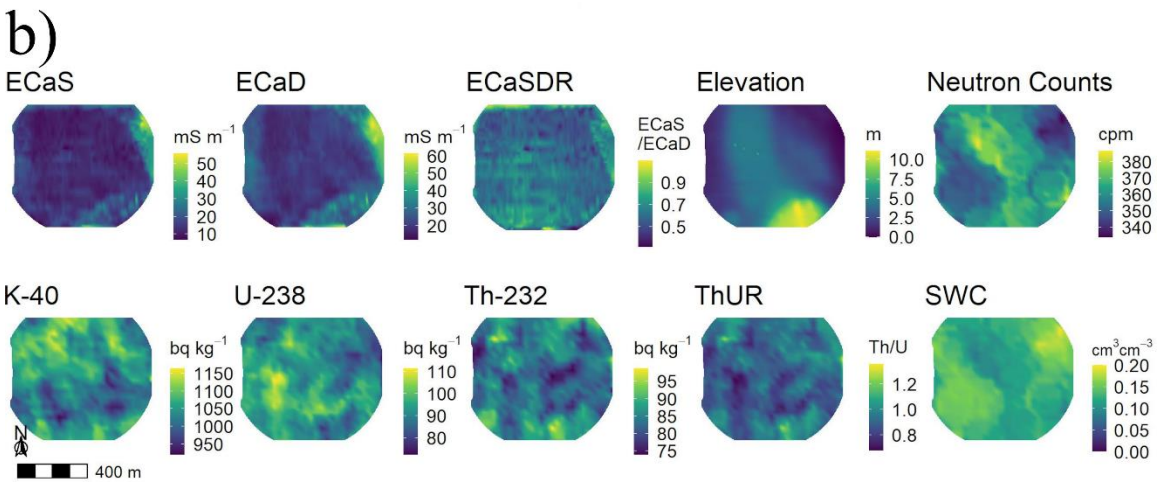

Figure 2.3b. Maps of geophysical data estimated by kriging at site 2. Shown are shallow apparent bulk electrical conductivity (ECaS), deep apparent bulk electrical conductivity (ECaD), ratio of shallow to deep apparent bulk electrical conductivity (ECaSDR), relative elevation, neutron counts, potassium (K-40), uranium (U-238), thorium (Th-232), ratio of thorium to uranium (ThUR), and soil water content estimated from neutron counts (SWC).

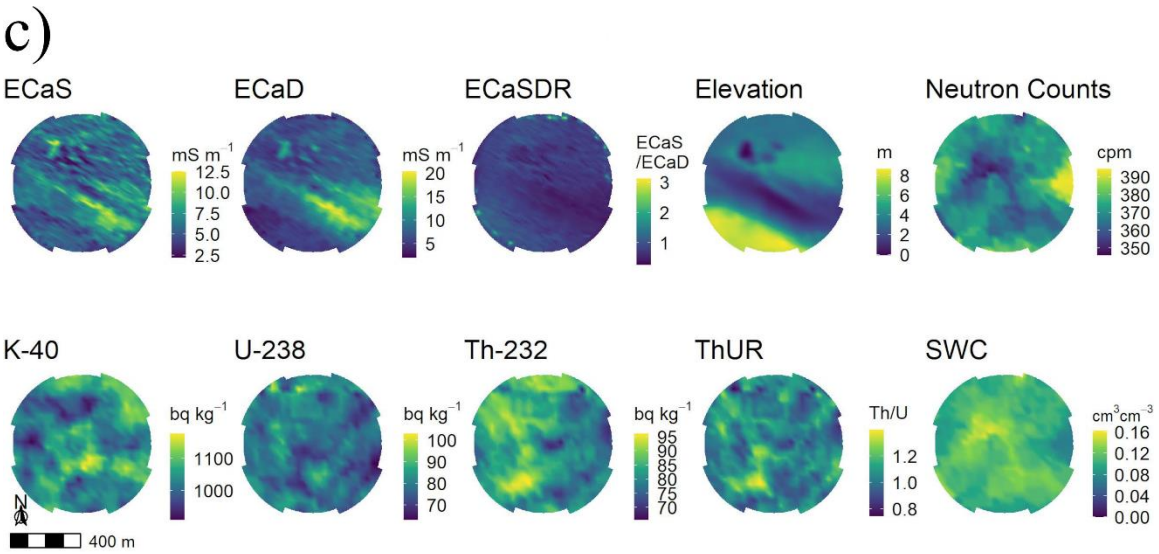

Figure 2.3c. Maps of geophysical data estimated by kriging at site 3. Shown are shallow apparent bulk electrical conductivity (ECaS), deep apparent bulk electrical conductivity (ECaD), ratio of shallow to deep apparent bulk electrical conductivity (ECaSDR), relative elevation, neutron counts, potassium (K-40), uranium (U-238), thorium (Th-232), ratio of thorium to uranium (ThUR), and soil water content estimated from neutron counts (SWC).

Table 2.2. Mean and uncertainties are reported for measured apparent bulk electrical conductivity (ECaS), deep apparent bulk electrical conductivity (ECaD), elevation, neutron counts (NC), K-40, U-238, Th-232 at all three sites. The uncertainty reported for variables with * is the instrument uncertainty.

Site	ECaS (mS m^{-1})*	ECaD (mS m^{-1})*	Elev (m)*	NC (cpm)
1	18.25 ± 0.25	18.99 ± 0.25	4.42 ± 0.02	390.86 ± 19.77
2	14.78 ± 0.25	23.69 ± 0.25	3.54 ± 0.02	359.77 ± 18.97
3	6.13 ± 0.25	8.24 ± 0.25	3.60 ± 0.02	371.47 ± 19.27
	K-40 (bq kg^{-1})	**U-238 (bq kg^{-1})**	**Th-232 (bq kg^{-1})**	
1	1016.54 ± 90.0	69.69 ± 12.27	81.90 ± 9.83	
2	1048.29 ± 94.05	91.75 ± 12.91	84.54 ± 10.22	
3	1044.39 ± 91.98	78.30 ± 12.55	81.92 ± 9.99	

2.3.2 Soil sampling

Descriptive statistics of sampled soil properties for the 0 – 0.30 m depth interval are given in Table 2.3 (summaries of remaining depth intervals in supplemental materials).

Table 2.3. Soil sample descriptive statistics from each of the field sites for 0 – 0.30 m. Data for depth intervals of 0.30 – 0.6m and 0.61 – 0.91m is available in supplemental materials. Soil properties reported are: pH, electrical conductivity (EC), cation exchange capacity (CEC), bulk density (BD), percent organic matter (OM), available water capacity (AWC), percent sand, percent silt, and percent clay. Summary statistics are the maximum (Max), minimum (Min), standard deviation (SD) and mean.

Property	Site	Max	Min	SD	Mean
pH	1	7.8	5.3	0.85	6.2
EC (mmhos cm^{-1})	1	0.38	0.13	0.085	0.24
OM (%)	1	3.5	0.3	1.1	2
CEC (meq $100g^{-1}$)	1	75	16	20	45
BD (g cm^{-3})	1	1.6	1.3	0.08	1.4
AWC (cm cm^{-1})	1	0.13	0.027	0.035	0.081
Sand (%)	1	94	55	14	72
Silt (%)	1	26	1	8.9	16
Clay (%)	1	21	5	5.8	12
pH	2	7.9	6.7	0.34	7.1
EC (mmhos cm^{-1})	2	0.85	0.51	0.11	0.69
OM (%)	2	4.4	1.8	0.82	3
CEC (meq $100g^{-1}$)	2	87	35	12	59
BD (g cm^{-3})	2	1.6	1.3	0.081	1.5
AWC (cm cm^{-1})	2	0.16	0.072	0.028	0.11
Sand (%)	2	77	43	9.1	66
Silt (%)	2	41	14	6.7	22
Clay (%)	2	17	7	3	11
pH	3	7.4	6.3	0.42	6.9
EC (mmhos cm^{-1})	3	0.32	0.21	0.039	0.26
OM (%)	3	5.1	2.3	0.69	3.1
CEC (meq $100g^{-1}$)	3	71	33	10	48
BD (g cm^{-3})	3	1.6	1.3	0.087	1.4
AWC (cm cm^{-1})	3	0.14	0.051	0.023	0.091
Sand (%)	3	78	52	7.3	69
Silt (%)	3	33	15	5.2	22
Clay (%)	3	15	7	2.4	9.7

Sample counts at site 3 were reduced to nine samples in the 0.30 – 0.61m interval and seven samples in the 0.61 – 0.91m interval for various reasons such as gravel, pooled sample length less than the desired minimum of 15 cm, or in one case a length recording

uncertainty. Correlations between sampled soil properties and geophysical layers are shown in Figure 2.4.

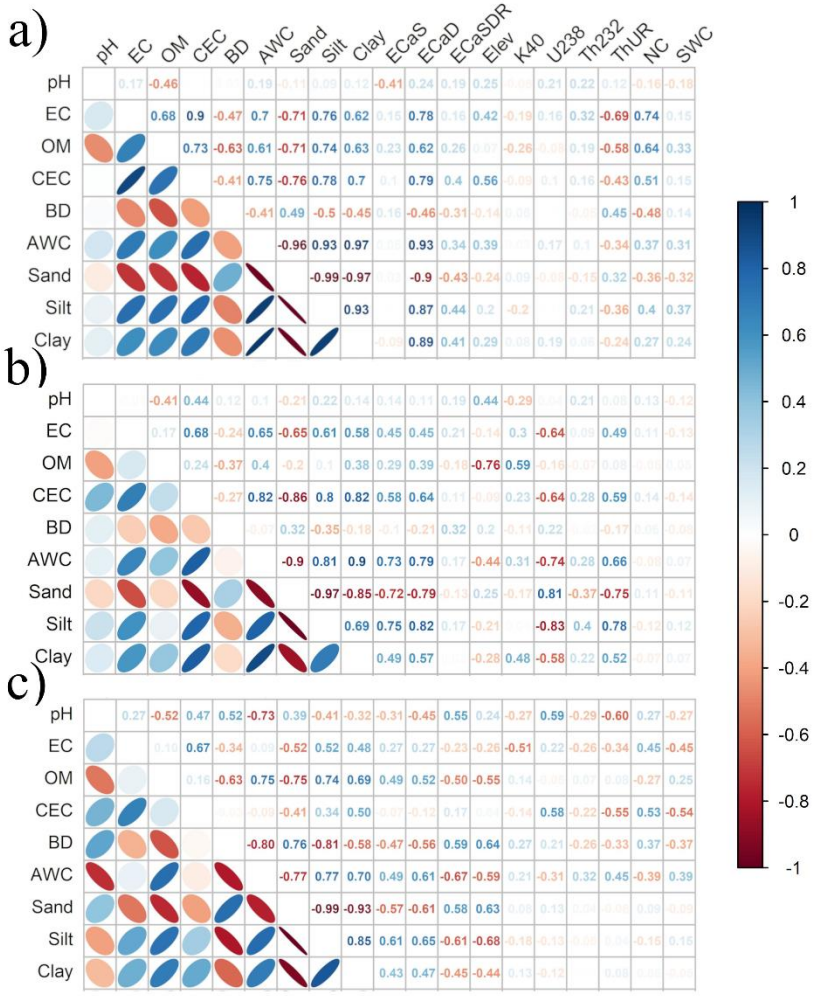

Figure 2.4. Correlations in the 0 – 0.30 m depth interval between soil properties and the log base 10 of geophysical data at site 1 (a), site 2 (b), and site 3 (c). Full correlation matrices of all depths are in supplemental materials.

Linear correlations between soil properties and geophysical data varied among sites and soil depths. The EMI data (ECaS, ECaD, and ECaSDR) was most often at least moderately correlated ($|r| > .5$) with soil properties compared to the other data types. Across all three sites, ECaS was most consistently correlated with percent sand, silt, and clay for the 0 – 0.30 m sampling interval, with correlation coefficients ranging from r =

.47 to r = .73. A strong correlation coefficient of r = .93 existed at site 1 between ECaSDR and AWC. Beyond the EMI data, correlations with other sensor data were more sporadic, such as the strong correlation between elevation and organic matter at site 2 (r = -.76) and moderate correlation between elevation and organic matter at site 3 (r = -.55). Elevation was also moderately correlated with bulk density, available water capacity, sand, and silt (r = .64, -.59, .63, -.68, respectively). K-40 was moderately correlated with EC and CEC in the 0. – 0.30 m depth interval at site 1 (r = .42, .56, respectively). At site 1 in the 0.61 – 0.91 m depth interval, U-238 and Th-232 were correlated with AWC, sand, silt, and clay with absolute value of correlation coefficients between r = .45 and r = .58. U-238 and Th-232 also had a moderate to strong correlation in the 0.61 – 0.91 m interval at site 1 with EC, OM, and BD, with absolute value of correlation coefficients between .53 and .83. U-238 had a moderate to strong correlation with texture, CEC, and AWC at site 2. The only noteworthy radionuclide correlations at site 3 were r = .58 and r = .59 for U-238 with CEC and pH, respectively. SWC was moderately correlated with EC, CEC, and organic matter at site 1, and was also moderately correlated with CEC at site 3.

2.3.4 Multiple Linear Regression Results

The number of soil properties and depth interval pairs (27 possible) that could be modeled by multiple linear regression with R^2_{pred} close to .5 (greater than .4) was 13, 14, and 6 at sites 1, 2, and 3, respectively (Table 2.4). The depth interval most often modeled successfully was 0 – 0.30 m. ECaS, U-238, neutron counts, and elevation were eliminated as possible predictor variables at site 1 to reduce multicollinearity. At site 2, ECaS, Th-232, and neutron counts were eliminated as possible predictor variables. At site 3, ECaS,

ECaD, ThUR, and neutron counts were excluded from prediction. Plots of residuals vs. fitted values showed minor heteroscedasticity in some CEC, EC, and pH models, but no correction was attempted. Only models with the lowest RMSEP for each soil property and depth pair are reported in Table 2.4. An exhaustive model summary is available in supplemental R code document.

Table 2.4. Multiple linear regression models with lowest root mean square error of prediction (RMSEP), where models with R^2_{pred} greater than 0.4 are underlined. Minimum (Min), maximum (Max), standard deviation (SD), mean, RMSEP, and R-squared of prediction (R^2_{pred}) are given. Response variables are pH, electrical conductivity (EC; mmhos cm^{-1}), cation exchange capacity (CEC; meq $100g^{-1}$), bulk density (BD; g cm^{-3}), percent organic matter (OM), available water capacity (AWC; cm cm^{-1}), percent sand, percent silt and percent clay. Predictor variables are shallow apparent bulk electrical conductivity (ECaS), deep apparent bulk electrical conductivity (ECaD), ratio of shallow to deep apparent bulk electrical conductivity (ECaSDR), potassium (K40), uranium (U238), thorium (Th232), ratio of thorium to uranium (ThUR), and soil water content from cosmic-ray neutron probe (SWC). Model descriptions assume that an intercept is also included.

Site	Model	Depth (m)	Min	Max	SD	Mean	RMSEP	R^2_{pred}
1	pH ~ ECaD	0 – 0.30	5.2	7.2	0.44	6	0.86	0.02
	pH ~ ECaD + SWC	0.30 – 0.61	5.2	7.8	0.47	6.2	0.57	0.21
	pH ~ ECaD + SWC	0.61 – 0.91	5.2	8.4	0.47	7	0.41	0.34
	EC ~ ECaSDR + SWC	0 – 0.30	0	0.36	0.065	0.24	0.055	0.58
	EC ~ ECaSDR	0.30 – 0.61	0.11	0.37	0.056	0.25	0.11	0.14
	EC ~ Th232 + ThUR	0.61 – 0.91	0	0.87	0.15	0.29	0.18	0.3
	CEC ~ ECaSDR + K40	0 – 0.30	1.6	77	14	44	13	0.58
	CEC ~ ECaSDR + K40	0.30 – 0.61	17	75	12	49	22	0.12
	CEC ~ Th232 + ThUR	0.61 – 0.91	2.4	89	15	38	13	0.58
	BD ~ ECaD + SWC	0 – 0.30	1.3	1.8	0.06	1.5	0.072	0.21
	BD ~ ECaSDR + Th232	0.30 – 0.61	1.3	1.7	0.056	1.5	0.076	0.2
	BD ~ K40 + SWC	0.61 – 0.91	1.4	1.8	0.098	1.6	0.12	0.35
	OM ~ ECaSDR	0 – 0.30	0.51	3.1	0.57	1.9	0.91	0.27
	OM ~ Th232 + ThUR	0.30 – 0.61	0.13	5.4	0.46	1.5	0.69	0.24
	OM ~ Th232 +ThUR	0.61 – 0.91	0	3.3	0.5	1.1	0.5	0.46

	AWC ~ ECaSDR	0 – 0.30	0.02	0.14	0.027	0.08	0.014	0.83
	AWC ~ ECaD + ECaSDR	0.30 – 0.61	0.02	0.16	0.035	0.092	0.033	0.44
	AWC ~ ECaD + Th232	0.61 – 0.91	0.02	0.21	0.046	0.094	0.03	0.62
	Sand ~ ECaSDR	0 – 0.30	49	97	11	72	6.9	0.75
	Sand ~ ECaSDR + K40	0.30 – 0.61	40	97	13	70	13	0.53
	Sand ~ Th232 + SWC	0.61 – 0.91	26	97	15	75	16	0.34
	Silt ~ ECaSDR	0 – 0.30	0	29	6.5	16	4.7	0.7
	Silt ~ ECaSDR	0.30 – 0.61	0	28	6.2	15	7.9	0.38
	Silt ~ Th232 + SWC	0.61 – 0.91	0	33	6.5	12	6.1	0.42
	Clay ~ ECaSDR + SWC	0 – 0.30	2	35	4.4	12	2.6	0.78
	Clay ~ ECaSDR + K40	0.30 – 0.61	2	30	6.7	15	6.7	0.53
	Clay ~ Th232 + SWC	0.61 – 0.91	2	35	8.1	14	9.9	0.25
2	pH ~ ECaD + Elev	0 – 0.30	6.1	7.9	0.18	7	0.3	0.18
	pH ~ K40	0.30 – 0.61	7.3	8.4	0.25	7.8	0.23	0.16
	pH ~ ThUR	0.61 – 0.91	7.5	8.4	0.11	8.2	0.28	0.011
	EC ~ ECaSDR + U238	0 – 0.30	0.89	1.5	0.12	1.2	0.095	0.25
	EC ~ ECaSDR + ThUR	0.30 – 0.61	0.46	1.7	0.18	1.1	0.13	0.13
	EC ~ ECaD + K40	0.61 – 0.91	0	1.5	0.3	0.29	0.15	0.45
	CEC ~ ECaD + SWC	0 – 0.30	35	95	9.2	67	10	0.25
	CEC ~ ECaD + Elev	0.30 – 0.61	1	95	15	49	14	0.32
	CEC ~ ECaD + K40	0.61 – 0.91	11	95	18	50	16	0.11
	BD ~ ECaD + ECaSDR	0 – 0.30	1.5	1.8	0.087	1.7	0.08	0.05
	BD ~ ECaD + K40	0.30 – 0.61	1.1	1.8	0.16	1.5	0.074	0.56
	BD ~ ECaD	0.61 – 0.91	1.4	1.8	0.1	1.6	0.098	0.30
	OM ~ Elev + SWC	0 – 0.30	2.6	8	0.93	4.5	0.51	0.61
	OM ~ ECaD + ECaSDR	0.30 – 0.61	0	1.7	0.32	0.22	0.41	0.51
	OM ~ ECaD	0.61 – 0.91	0	1.6	0.41	0.61	0.22	0.65
	AWC ~ ECaD + U238	0 – 0.30	0.1	0.23	0.024	0.16	0.017	0.63
	AWC ~ ECaD	0.30 – 0.61	0.035	0.17	0.037	0.064	0.023	0.63
	AWC ~ ECaD + Elev	0.61 – 0.91	0.035	0.23	0.024	0.05	0.038	0.42

	Sand ~ ECaD + U238	0 – 0.30	19	66	8	46	5.3	0.66
	Sand ~ ECaD + ECaSDR	0.30 – 0.61	52	96	9.8	90	12	0.48
	Sand ~ ECaD + Elev	0.61 – 0.91	40	96	8.8	86	8.3	0.49
	Silt ~ ECaD + U238	0 – 0.30	23	58	6.1	37	3.6	0.71
	Silt ~ ECaD + Elev	0.30 – 0.61	2	51	8	11	7.9	0.37
	Silt ~ ECaD + Elev	0.61 – 0.91	2	47	6.3	9.9	7.4	0.33
	Clay ~ ECaD + K40	0 – 0.30	1	17	2.5	8.6	2.6	0.29
	Clay ~ ECaD + ECaSDR	0.30 – 0.61	1	15	2.1	2.1	3.4	0.66
	Clay ~ ECaD + ThUR	0.61 – 0.91	1	17	3.4	5.8	2.3	0.57
3	pH ~ U238 + Th232	0 – 0.30	6.3	7.8	0.22	6.9	0.36	0.25
	pH ~ ECaSDR + SWC	0.30 – 0.61	6.3	8.4	0.28	7.1	0.29	0.39
	pH ~ ECaSDR	0.61 – 0.91	6.3	8.4	0.33	7.3	0.41	0.3
	EC ~ Elev + SWC	0 – 0.30	0.16	0.42	0.032	0.26	0.03	0.37
	EC ~ ECaSDR	0.30 – 0.61	0.25	0.42	0.016	0.35	0.77	0.84
	EC ~ K40 + U238	0.61 – 0.91	0	0.31	0.069	0.1	0.081	0.32
	CEC ~ Elev + SWC	0 – 0.30	23	73	7.6	47	9.1	0.2
	CEC ~ U238 + SWC	0.30 – 0.61	0	39	6.5	22	10	0.26
	CEC ~ K40 + U238	0.61 – 0.91	0	71	16	25	17	0.35
	BD ~ ECaSDR + Th232	0 – 0.30	1.3	1.7	0.054	1.4	0.075	0.25
	BD ~ ECaSDR	0.30 – 0.61	1.3	1.9	0.067	1.5	0.13	0.056
	BD ~ SWC	0.61 – 0.91	1.6	1.7	0.021	1.7	0.11	0.084
	OM ~ ECaSDR	0 – 0.30	1.2	4.8	0.34	3.2	0.69	0.039
	OM ~ U238	0.30 – 0.61	0.037	1.8	0.23	1	0.62	0.038
	OM ~ K40 + U238	0.61 – 0.91	0	2.3	0.5	0.71	0.5	0.45
	AWC ~ ECaSDR + Th232	0 – 0.30	0.04	0.16	0.017	0.094	0.017	0.46
	AWC ~ U238	0.30 – 0.61	0.04	0.21	0.029	0.11	0.05	0.21
	AWC ~ SWC	0.61 – 0.91	0.052	0.2	0.024	0.12	0.064	0.0012
	Sand ~ ECaSDR	0 – 0.30	49	92	4.2	67	6.8	0.12
	Sand ~ Th232	0.30 – 0.61	78	87	1.6	82	5.9	0.000064
	Sand ~ ECaSDR + K40	0.61 – 0.91	55	97	7.3	83	8.9	0.22
	Silt ~ Elev	0 – 0.30	17	38	2.4	21	4.6	0.22
	Silt ~ Elev	0.30 – 0.61	11	21	0.71	12	5	0.039
	Silt ~ ECaSDR + K40	0.61 – 0.91	1	30	5.3	10	6.1	0.25
	Clay ~ ECaSDR	0 – 0.30	3.6	15	1.1	9.9	2.4	0.012
	Clay ~ ECaSDR + SWC	0.30 – 0.61	0	12	1.4	6.7	2.3	0.031

Clay ~ Elev + K40	0.61 – 0.91	0.97	23	2.1	5.8	3.7	0.071

At site 1, pH models for 0.30 – 0.61 m and 0.61 – 0.91 m with K-40, Th-232, or ThUR as predictors had R^2_{pred} > .5 but p-values greater than 0.65. Significant (p-value < .01) predictor variables for the EC models in the 0 – 0.30 m interval were ECaSDR, ThUR, and SWC. A significant (p-value < 0.01) model for OM in the 0.61-0.91 m interval with R^2_{pred} was predicted with Th-232 and ThUR. All possible predictive variable combinations involving ECaSDR at site 1 were able to predict AWC from 0 – 0.30 m with R^2_{pred} greater than .8. The p-values of the secondary predictor variable coefficients for AWC models range from .26 to .95 while the p-values of the ECaSDR coefficients were between 3.61×10^{-6} and 5.48×10^{-7}. Models for 0 – 0.30 m AWC at site 1 that did not contain ECaSDR had large overall p-values (p-value > .15). ECaD was a significant predictor for AWC in the 0.30 - 0.61 m and 0.61 - 0.91 m depth intervals. Models of 0 – 0.30 m sand, silt, and clay at site 1 predicted with ECaSDR in any combination all achieved an R^2_{pred} greater than .65 and overall p-values < .01.

At site 2, significant models with R^2_{pred} > .5 predicted bulk density with ECaD as the primary predictor and K-40 or ThUR as the secondary predictors. Elevation with SWC and elevation with K-40 predicted organic matter with R^2_{pred} > .5 in the 0 – 0.30 m interval. For the organic matter in the 0.61 – 0.91 m interval, all models including ECaD were significant and achieved R^2_{pred} > .5. All models at site 2 that included ECaD as a predictor, excluding the ECaD and elevation model, were significant and achieved R^2_{pred} greater than .48 for 0 – 0.30 m AWC. The 0.30 – 0.61 m AWC was also well-predicted

with all models containing ECaD; the lowest R^2_{pred} was .53. Behind ECaD, the next best predictors for the first and second depth intervals of AWC were U-238 (R^2_{pred} = .42) and K-40 (R^2_{pred} = .37), respectively. Sand models for 0 – 0.30 m with R^2_{pred} > .5 were predicted with ECaD and U-238, elevation, or ECaSDR. All clay models for 0.30 – 0.61 m and 0.61 – 0.91 m that included ECaD achieved R^2_{pred} values between .45 and .66. K-40 alone predicted clay with R^2_{pred} of .47 and .61 for the 0.30 – 0.61 m and 0.61 – 0.91 m intervals, respectively.

One soil property was predicted at site 3 with R^2_{pred} greater than .50. EC was predicted by elevation in the 0.30 – 0.61 m interval with R^2_{pred} = 0.84, but the model was not significant (p-value = 0.94). A model for AWC in the 0.0 – 0.30 m depth interval with Th-232 and ECaSDR as predictors achieved an R^2_{pred} of .46. Organic matter was predicted with K-40 and U-238 from 0.61 – 0.91 m with an R^2_{pred} of .45. For all the soil properties combined, U-238 and elevation were the predictors with p-values most frequently less than .01. Overall p-values were less than .01 for 24 models at site 3 compared to 82 and 147 models at sites 1 and 2, respectively.

2.3.5 Spatial Predictions of Soil Properties

Underlined models in Table 2.4 were mapped spatially in Figures 2.5 – 2.7.

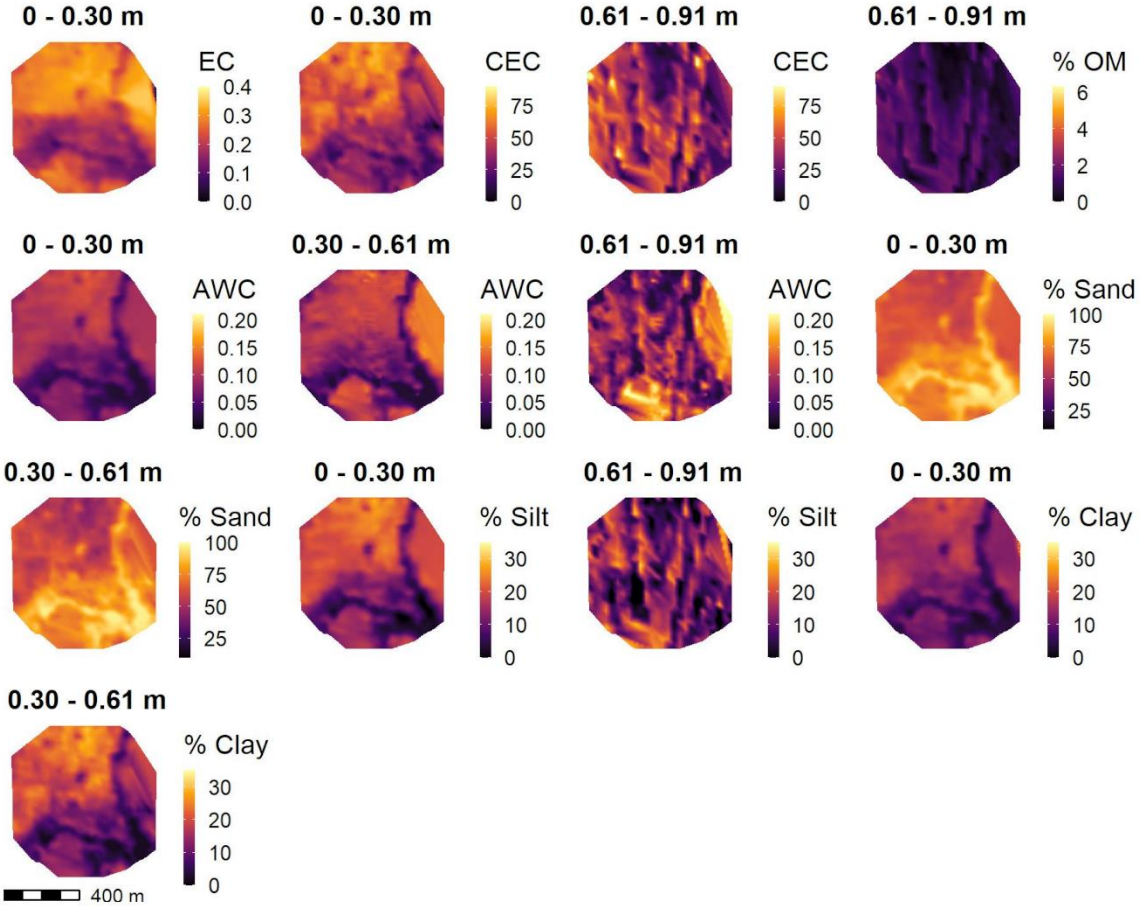

Figure 2.5. The underlined models in Table 4 are mapped in space at site 1. Soil properties predicted are pH, electrical conductivity (EC; mmhos cm^{-1}), cation exchange capacity (CEC; meq $100g^{-1}$), bulk density (BD; g cm^{-3}), percent organic matter (OM), available water capacity (AWC; cm cm^{-1}), percent sand, percent silt and percent clay.

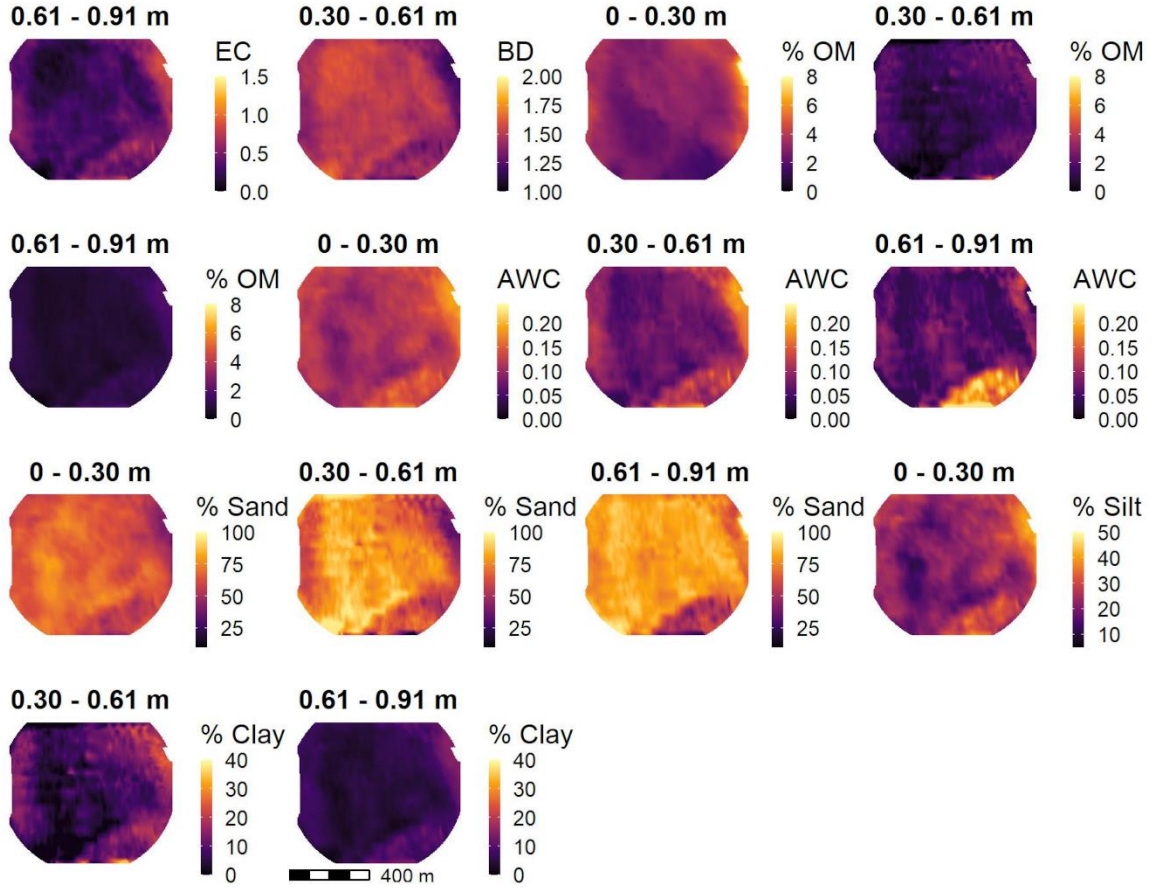

Figure 2.6. The underlined models in Table 2.4 are mapped in space at site 2.

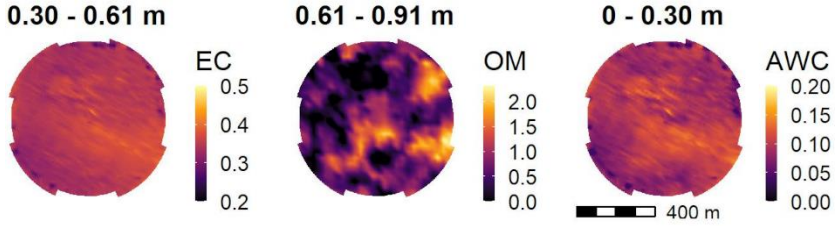

Figure 2.7. The underlined models in Table 2.4 are mapped in space at site 3.

When comparing predictions to uncertainty thresholds (Table 2.1), 11 models pass at site 1, 16 at site 2, and 14 at site 3. Despite meeting uncertainty thresholds, most of the models at Site 3 still have a low R^2_{pred}, showing that the variation within the field may be too low for a spatial prediction to add any useful information to the mean. There were

also model cases where R^2_{pred} was greater than .5 but the uncertainty was too high (Table 2.4). Soil properties that were predicted at site 1 with both an R^2_{pred} > .5 and low enough uncertainty were EC, AWC, silt, and clay. At site 2, bulk density, organic matter, AWC, silt, and clay were predicted with R^2_{pred} > .5 and acceptable uncertainty. AWC was the only soil property predicted at site 3 with acceptable uncertainty and R^2_{pred} close to .5 (R^2_{pred}= .46).

2.4 Discussion

Because a number of the statistical models produced favorable R^2_{pred} values, coupling of geophysical surveys with a small number of soil core samples with MLR proved to be a reasonable strategy that invites further development. The small number of soil samples (15) collected at each site in this study was on par with the reality that measuring soil core properties will always be time-consuming and expensive. Incorporating geophysical data allowed us to infer how the measured soil properties vary across a field with much smaller collection and analysis time than would be required for extensive grid soil sampling.

Our results agree with the inconsistent predictor-response relationships presented by Rodrigues Jr. et al. (2015) and Wong and Harper (1999). The models trained at each of the three sites were also applied to the other two sites to explore potential for a universal calibration among our sites. However, 74% of the resulting predictions had more variance between the predicted soil properties and the sample mean than between the observed soil properties and the sample mean. The results indicate that local

calibration is still needed, and that further work needs to be done to approach a universal calibration for these sites similar to Rodrigues Jr. et al. (2015). At the sites in this study, EMI (ECaS, ECaD, ECaSDR) appeared to be the most useful geophysical layer. While GRS (K-40, U-238, Th-232) and CRNS (neutron counts, SWC) data added some information, the correlations with soil properties were not uniform across sites or soil depth intervals, and the model coefficients for GRS and CRNS variables were usually less significant than those of EMI when used as joint predictors.

These differences in the sensors' predictive performance raise a short discussion of the sources of error and bias introduced by their differences in measurement frequency and sample volume. Since all sensors were traveling at the same speed and the EMI sensor had the highest sampling frequency at one measurement per second, the distance between consecutive EMI measurements was smaller (2.78 m) than the distance between consecutive GRS and CRNS measurements (27.78 m and 166.78 m, respectively). The fact that more EMI data points were collected than GRS and CRNS data points and that EMI soundings are most similar in scale to soil samples may explain why EMI generally performed as the best predictor in our models. However, despite the better fit in scale between EMI data and soil samples, Gibson and Franz (2011) found that CRNS was more strongly correlated with soil hydraulic properties than EMI. The sample volume for the GRS and CRNS sensors (circles with radii roughly 24 m and 200 m, respectively) are large enough the capture the information between the larger measurement spacings so that the same ground is covered even though fewer measurements are taken. At the same time, both the GRS and CRNS sensors are more sensitive to the ground volume closer to the detector. In addition to differences in horizontal spatial scale, the authors

acknowledge errors introduced by differences vertical scales of the soil sampling depth intervals and the sensing depths of the geophysical sensors. Each sensor has a slightly different sensitivity function with depth below the soil surface, and inversion of geophysical data was not attempted for the sake of simplicity in future practical use. We refer the reader to other papers that have studied inversion of EMI data (Callegary et al., 2007, Piikki et al., 2014) and the vertical and horizontal support volume of CRNS and GRNS sensors more in-depth (Köhli et al., 2015; van der Veeke et al., 2021).

For soil cores in this study, uniform sampling combined with ECaD, SSURGO, and elevation information was used to intuitively select informative locations for a few soil samples. The authors acknowledge that consideration of ECaD data in selection of soil sample locations (and not GRS and CRNS data) introduces bias toward EMI data as a successful predictor in soil property models. Future work could examine the relative success of EMI, GRS, and CRNS data when all three sensor data types are formally considered in soil sample selection. Despite introduction of bias toward certain predictive data types, development of intelligent sampling strategies based on elevation, SSURGO zones, and geophysical surveys is essential for maximizing the potential of MLR for situations with sampling constraints. One situation with limited soil sample size is the soil organic carbon storage industry. For verification of soil organic carbon storage, practical recommendation by the Food and Agriculture Organization of the United Nations (FAO) is currently one composite sample per ten ha (FAO, 2020). This would be equivalent to collecting only five soil samples per site in this study. The first basic approach the FAO recommends is stratified simple random sampling, where at least three strata - or zones - are determined by dividing the area of interest equally. The second approach is direct

stratified sampling, where at least three strata are identified from previous information such as apparent bulk electrical conductivity maps. In both methods at least three composite soil samples are randomly collected in each stratum. Clearly, selecting representative sample locations of soil organic carbon highly important for accurately understanding carbon storage and enabling the carbon credit industry to become lucrative for producers. A promising approach to intelligent selection of sample locations is to employ k-means clustering of geophysical and other available data. For example, van Arkel and Keleita (2014) used k-means clustering of EMI and topography data to select critical soil moisture sampling locations for estimation of mean field-scale soil moisture and concluded that the approach was a good alternative to other selection methods because it performed nearly as well or better without the need for extensive pre-sampling. In a hypothetical method, k-means clustering of ECa and elevation data in feature space would create map zones within which centroidal voronoi tessellations could be calculated with Lloyd's algorithm (Lloyd, 1982). Sample locations would then be the centers of the voronoi tessellations within the different zones characterized by ECa and elevation. Extra constraints are required to ensure that k-means clusters in feature space are mapped to zones that are concave, connected, and large enough in real space.

Although the MLR predictions were moderately successful, we also acknowledge limitations in our predicting capabilities. At site 3, we were surprised to find that none of the significant MLR models met $R^2_{pred} > .5$. Probable cause of failure was low variability within site 3 to the best of our knowledge. In addition, soils at site 3 are highly disturbed because the site has been previously used for gravel production due to its proximity to the James River. The variance in ECaD at site 3 was 10.55 mS m^{-1}

compared to variances of 58.32 and 47.55 mS m^{-1} at sites 1 and 2, respectively. Furthermore, sampled soil properties at site 3 also tended to have a lower standard deviation than the measured soil properties at sites 1 and 2 (Table 2.3). Due to the low variability, the best statistical inferences for soil properties at site 3 were the sample means instead of regression model predictions. In addition to within-field variability, transient soil temperature and soil moisture may have also influenced EMI performance at the different sites. Brevik et al. (2006) found that the difference in ECa readings between different soils decreased as soil moisture decreased. Gibson and Franz (2018) found that the use of multiple mapping times combined with Empirical Orthogonal Functions could reduce the transient effects of soil temperature and soil moisture on EMI and CRNS data. The authors are not confident that type of parent material is a cause of statistical modeling failure. Site 3 material does appear to be less weathered since gravelly sands are dominant below about 0.5 m, but the parent materials at sites 2 and 3 are both river-deposited cross-bedded sand and plane-bedded gravel. However, collection of soil mineralogy data in the future could distinguish between quartz sands and potassium-feldspar sands to allow better interpretation of the gamma-ray data (Heggemann et al., 2017; Priori et al., 2014). Inclusion of soil mineralogy data in the models would likely improve the predictive ability of gamma-ray data at all three sites. Small sample size and non-linear relationships between predictor and response variables may have also limited MLR model performance, which typically improves with increased sample size (Khaledian and Miller, 2020).

In the future, the limitation of not knowing whether a site is a good candidate for linear regression may be overcome by examining readily available online data such as

elevation and SSURGO data. For instance, Lo et al. (2016) utilized SSURGO data to calculate the field-averaged amount of undepleted available soil water in the root zone under conventional irrigation by examining differences in root zone water holding capacity among soil units. Soil water at the end of the growing season above a critical management threshold was considered undepleted, and Lo et al. used the field average amount of undepleted available soil water to estimate benefits of implementing variable rate irrigation for mining undepleted soil water through planned depletion. A similar approach based on variability in SURRGO data may be possible to estimate feasibility of multiple linear regression modeling at a given site. Another practical development required for implementation in precision agriculture is to compile evidence-based uncertainty targets for MLR predictions. Work needs to be done to determine the actual uncertainty level required in each soil property to make a variable management decision. It would also be beneficial to determine decision threshold values for certain treatments where there is a yes-no decision. These thresholds would be used to evaluate a statistical model's ability to differentiate a field into zones that are either below or above a given decision threshold. Finally, both GRS and CRNS require investment in data processing, whether through obtaining expert support in software use, purchasing sensors with embedded software, or spending extended time learning the details of the method. This time or monetary cost motivates a recommendation of whether GRS and CRNS data is worthwhile at future sites. Although further study is needed, GRS and CRNS data may not be essential at sites with similar pedology and variation to those in this study.

2.5 Conclusions

This paper contributes to understanding the usefulness of geophysical data types by introducing results from three new pedological and geographic settings in North Dakota, United States. Over half of the best soil property predictions were based on multiple data sources instead of data from a single sensor (Table 2.4). Statistical models at two of the three sites met expert opinion for uncertainty targets in variable management decision-making. It is unclear which geophysical data type is expected to be the best predictor a priori at a given location. Our predictions were site-specific, and models trained at one site performed very poorly at the other sites. Our understanding of sensor performance and its relationship to field conditions and sensor support volumes could be further refined by incorporation of more information such as soil mineralogy and spatial variability of soil property values. However, based on results from these sites with our simplistic method, the authors recommend prioritizing EMI surveys if geophysical data collection is limited to a single mapping effort and calibration soil samples are few.

2.6 Acknowledgement

We acknowledge the support from USDA National Institute of Food and Agriculture Foundational Program Cyber-physical systems (2019-67021-29312). T.E.F. and D.D.S acknowledge the financial support of the USDA National Institute of Food and Agriculture, Hatch project #s 1009760 and ND0140, respectively. Financial support was provided by the Joint FAO/IAEA Programme of Nuclear Techniques in Food and Agriculture through the Coordinated Research Project (CRP) D1.20.14 Enhancing

agricultural resilience and water security using Cosmic-Ray Neutron Sensor (2019–2024). The research presented is also a result of a joint study by USDA-NRCS North Dakota (under agreement #NR206633XXXXC001), North Dakota State University, and the University of Nebraska-Lincoln on irrigation water management and variable rate irrigation technologies; and was partially supported by the North Dakota Agricultural Experiment Station. We appreciate the equipment, time, and expertise for soil sampling provided by Jordaan Thompson-Larson, Erica Althoff, and others of the USDA-NRCS staff of North Dakota. We thank Sheldon Tuscherer, Dongqing Lin, and Mathew Blum for field and laboratory support. Mention of equipment and trade names is for information only and is not intended to constitute endorsement by the authors, their respective organizations, or the research sponsors, of one product to the exclusion of others available for similar purposes.

References

Abdu, H., Robinson, D. A., Seyfried, M., & Jones, S. B. (2008). Geophysical imaging of watershed subsurface patterns and prediction of soil texture and water holding capacity: GEOPHYSICAL IMAGING OF WATERSHED SUBSURFACE. *Water Resources Research*, *44*(4). https://doi.org/10.1029/2008WR007043

Andreasen, M., Jensen, K. H., Desilets, D., Franz, T. E., Zreda, M., Bogena, H. R., & Looms, M. C. (2017). Status and Perspectives on the Cosmic-Ray Neutron Method for Soil Moisture Estimation and Other Environmental Science Applications. *Vadose Zone Journal*, *16*(8), vzj2017.04.0086. https://doi.org/10.2136/vzj2017.04.0086

Bluemle, J. P. (1975). *Guide to the Geology of Southeastern North Dakota* (Educational Series 3). North Dakota Geological Survey.

Brevik, E. C., Fenton, T. E., & Lazari, A. (2006). Soil electrical conductivity as a function of soil water content and implications for soil mapping. *Precision Agriculture*, *7*(6), 393–404. https://doi.org/10.1007/s11119-006-9021-x

Caciolli, A., Baldoncini, M., Bezzon, G. P., Broggini, C., Buso, G. P., Callegari, I., Colonna, T., Fiorentini, G., Guastaldi, E., Mantovani, F., Massa, G., Menegazzo, R., Mou, L., Rossi Alvarez, C., Shyti, M., Zanon, A., & Xhixha, G. (2012). A new

FSA approach for in situ γ ray spectroscopy. *Science of the Total Environment*, *414*, 639–645.

Carroll, T. R. (1981). AIRBORNE SOIL MOISTURE MEASUREMENT USING NATURAL TERRESTRIAL GAMMA RADIATION: *Soil Science*, *132*(5), 358–366. https://doi.org/10.1097/00010694-198111000-00006

Castrignanò, A., Wong, M. T. F., Stelluti, D., De Benedetto, D., & Sollitto, D. (2012). Use of EMI, gamma-ray emission and GPS height as multi-sensor data for soil characterisation. *Geoderma*, *175–176*, 78–89. http://dx.doi.org/10.1016/j.geoderma.2012.01.013

Desilets, D., Zreda, M., & Ferré, T. P. A. (2010). Nature's neutron probe: Land surface hydrology at an elusive scale with cosmic rays: NATURE'S NEUTRON PROBE. *Water Resources Research*, *46*(11). https://doi.org/10.1029/2009WR008726

Dierke, C., & Werban, U. (2013). Relationships between gamma-ray data and soil properties at an agricultural test site. *Geoderma*, *199*, 90–98. https://doi.org/10.1016/j.geoderma.2012.10.017

Dualem Inc. (2013). DUALEM-21S User' s Manual. Dualem Inc. www.dualem.com

Finkenbiner, C. E., Franz, T. E., Gibson, J., Heeren, D. M., & Luck, J. (2019). Integration of hydrogeophysical datasets and empirical orthogonal functions for improved irrigation water management. *Precision Agriculture*, *20*(1), 78–100. https://doi.org/10.1007/s11119-018-9582-5

Florinsky, I. V., Eilers, R. G., Manning, G. R., & Fuller, L. G. (2002). Prediction of soil properties by digital terrain modelling. *Environmental Modelling and Software*, *17*(3), 295–311. https://doi.org/10.1016/S1364-8152(01)00067-6

Food and Agriculture Organization of the United Nations. (2020). *A protocol for measurement, monitoring, reporting and verification of soil organic carbon in agricultural landscapes—GSOC-MRV Protocol*. FAO. https://doi.org/10.4060/cb0509en

Franz, T. E., Loecke, T. D., Burgin, A. J., Zhou, Y., Le, T., & Moscicki, D. (2017). Spatiotemporal predictions of soil properties and states in variably saturated landscapes. *Journal of Geophysical Research: Biogeosciences*, *122*(7), 1576–1596. https://doi.org/10.1002/2017JG003837

Franz, T. E., Wang, T., Avery, W., Finkenbiner, C., & Brocca, L. (2015). Combined analysis of soil moisture measurements from roving and fixed cosmic ray neutron probes for multiscale real-time monitoring. *Geophysical Research Letters*, *42*(9), 3389–3396. https://doi.org/10.1002/2015GL063963

Gardner, W. H. (1986). Water Content. In A. Klute (Ed.), *Methods of Soil Analysis: Part 1 Physical and Mineralogical Methods* (2nd ed., pp. 493–544). Soil Science Society of America, American Society of Agronomy. https://doi.org/10.2136/sssabookser5.1.2ed.c21

Gibson, J., & Franz, T. E. (2018). Spatial prediction of near surface soil water retention functions using hydrogeophysics and empirical orthogonal functions. *Journal of Hydrology*, *561*, 372–383. https://doi.org/10.1016/j.jhydrol.2018.03.046

IAEA. (2003). *Guidelines for radio element mapping using gamma ray spectrometry data* (No. 1363; Technical Documents). International Atomic Energy Agency.

Hamrita, T. K., Tollner, E. W., & Schafer, R. L. (2000). Toward Fulfilling the Robotic Farming Vision: Advances in Sensors and Controllers for Agricultural Applications. *IEEE Transactions on Industry Applications*, *36*(4), 1026–1032.

Heggemann, T., Welp, G., Amelung, W., Angst, G., Franz, S. O., Koszinski, S., Schmidt, K., & Pätzold, S. (2017). Proximal gamma-ray spectrometry for site-independent in situ prediction of soil texture on ten heterogeneous fields in Germany using support vector machines. *Soil and Tillage Research*, *168*, 99–109. https://doi.org/10.1016/j.still.2016.10.008

Hendriks, P. H. G. M., Limburg, J., & de Meijer, R. J. (2001). Full-spectrum analysis of natural γ-ray spectra. *Journal of Environmental Radioactivity*, *53*(3), 365–380. https://doi.org/10.1016/S0265-931X(00)00142-9

Ji, W., Adamchuk, V. I., Chen, S., Biswas, A., Mat Su, A. S., Ismail, A., Gan, Q., & Shi, Z. (2019). Simultaneous measurement of multiple soil properties through proximal sensor data fusion: A case study. *Geoderma*, *341*, 111–128.

Khaledian, Y., & Miller, B. A. (2020). Selecting appropriate machine learning methods for digital soil mapping. *Applied Mathematical Modelling*, *81*, 401–418. https://doi.org/10.1016/j.apm.2019.12.016

Köhli, M., Schrön, M., Zreda, M., Schmidt, U., Dietrich, P., & Zacharias, S. (2015). Footprint Characteristics Revised for Field-Scale Soil Moisture Monitoring with Cosmic-Ray Neutrons. *Water Resources Research*, *51*(7), 5772–5790. https://doi.org/10.1002/2015WR017169

Lesch, S. M., Rhoades, J. D., & Corwin, D. L. (2000). *ESAP-95 Version 2.01R User Manual and Tutorial Guide* (USSL Research Report No. 146; p. 169). USDA - ARS.

Lloyd, S. (1982). Least squares quantization in PCM. *IEEE Transactions on Information Theory*, *28*(2), 129–137. https://doi.org/10.1109/TIT.1982.1056489

Lo, T., Heeren, D. M., Martin, D. L., Mateos, L., Luck, J. D., & Eisenhauer, D. E. (2016). Pumpage Reduction by Using Variable-Rate Irrigation to Mine Undepleted Soil Water. *Transactions of the ASABE*, *59*(5), 1285–1298. https://doi.org/10.13031/trans.59.11773

Mahmood, H. S. M., Hoogmoed, W. B., & van Henten, E. J. (2013). Proximal Gamma-Ray Spectroscopy to Predict Soil Properties Using Windows and Full-Spectrum Analysis Methods. *Sensors*, *13*, 16263–16280. https://doi.org/10.3390/s131216263

McBratney, A. B., Minasny, B., & Whelan, B. M. (2005). Obtaining 'useful' high-resolution soil data from proximally-sensed electrical conductivity/resistivity (PSEC/R) Surveys. In J. V. Stafford (Ed.), *Precision Agriculture '05: Proceedings of the 5th European Conference on Precision Agriculture*. Wageningen Academic Publishers. https://doi.org/10.3920/978-90-8686-549-9

North Dakota Agricultural Weather Network. (2021). Fargo: N. Dak. State Univ. Data retrieved from https://ndawn.ndsu.nodak.edu/

National Weather Service. (2021). North Dakota Climate Normals (1991-2020). Retrieved from https://ggweather.com/normals/ND91.html

O'Shaughnessy, S. A., Evett, S. R., Colaizzi, P. D., Andrade, M. A., Marek, T. H., Heeren, D. M., Lamm, F. R., & LaRue, J. L. (2019). Identifying Advantages and

Disadvantages of Variable Rate Irrigation: An Updated Review. *Applied Engineering in Agriculture*, *35*(6), 837–852. https://doi.org/10.13031/aea.13128

Piikki, K., Söderström, M., & Stenberg, B. (2013). Sensor data fusion for topsoil clay mapping. *Geoderma*, *199*, 106–116.

Piikki, K., Wetterlind, J., Söderström, M., & Stenberg, B. (2014). Constructing a layered electrical conductivity model using *k* nearest-neighbour predictions and a combination of two proximal sensors: A two-layer map of soil electrical conductivity. *European Journal of Soil Science*, *65*(6), 816–826. https://doi.org/10.1111/ejss.12201

Plume, K. (2021, April 28). Farmers struggle to break into booming carbon-credit market. *Reuters*. https://www.reuters.com/business/energy/farmers-struggle-break-into-booming-carbon-credit-market-2021-04-28/

Priori, S., Bianconi, N., & Costantini, E. A. C. (2014). Can γ-radiometrics predict soil textural data and stoniness in different parent materials? A comparison of two machine-learning methods. *Geoderma*, *226–227*, 354–364. https://doi.org/10.1016/j.geoderma.2014.03.012

Rodrigues Jr., F. A., Bramley, R. G. V., & Gobbett, D. L. (2015). Proximal soil sensing for Precision Agriculture: Simultaneous use of electromagnetic induction and gamma radiometrics in contrasting soils. *Geoderma*, *243–244*, 183–195. http://dx.doi.org/10.1016/j.geoderma.2015.01.004

Rossel, R. A. V., Taylor, H. J., & McBratney, A. B. (2007). Multivariate calibration of hyperspectral γ-ray energy spectra for proximal soil sensing. *European Journal of Soil Science*, *58*(1), 343–353. https://doi.org/10.1111/j.1365-2389.2006.00859.x

Shearer, S. A., & Ward, A. D. (1999). Site-Specific Farming: A Perspective on Information Needs, Benefits and Limitations. *Journal of Soil and Water Conservation*, 7.

Söderstrom, M., Sohlenius, G., Rodhe, L., & Piikki, K. (2016). Adaptation of regional digital soil mapping for precision agriculture. *Precision Agriculture*, *17*, 588–607.

Combs, S. M., & Nathan, M. V. (2015). Soil organic matter. In *Recommended Chemical Soil Test Procedures for the North Central Region. North Cent. Reg. Res. Publ. No. 221 (Rev.)*. Missouri Agric. Exp. Sta. SB 1001. Univ. of Missouri, Columbia MO.

Soil Survey Staff, Natural Resources Conservation Service, United States Department of Agriculture. Web Soil Survey. Available at https://websoilsurvey.nrcs.usda.gov/. (verified 5 April 2021).

State of North Dakota. 2020. NDGISHUB Surface Geology [Online]. Available at https://gishubdata-ndgov.hub.arcgis.com/datasets/NDGOV::ndgishub-surface-geology/explore?location=47.467472%2C-100.301489%2C7.56 (verified 16 June 2021).

State of North Dakota. 2020. NDGISHUB Bedrock Geology [Online]. Available at https://gishubdata-ndgov.hub.arcgis.com/datasets/ndgishub-bedrock-geology/explore?location=47.467545%2C-100.300898%2C7.56 (verified 16 June 2021).

State of North Dakota. 2020. NDGISHUB County Boundaries [Online]. Available at https://gishubdata-ndgov.hub.arcgis.com/datasets/ndgishub-county-

boundaries/explore?location=47.445467%2C-100.301699%2C7.56 (verified 16 June 2021).

Van Arkel, Z., & Kaleita, A. L. (2014). Identifying sampling locations for field-scale soil moisture estimation using K-means clustering. *Water Resources Research*, *50*(8), 7050–7057. https://doi.org/10.1002/2013WR015015

van der Klooster, E., van Egmond, F. M., & Sonneveld, M. P. W. (2011). Mapping soil clay contents in Dutch marine districtsusing gamma-ray spectrometry. *European Journal of Soil Science*, *62*(5), 743–753.

van der Veeke, S., Limburg, J., Koomans, R. L., Söderström, M., de Waal, S. N., & van der Graaf, E. R. (2021). Footprint and height corrections for UAV-borne gamma-ray spectrometry studies. *Journal of Environmental Radioactivity*, *231*. https://doi.org/10.1016/j.jenvrad.2021.106545

van Egmond, F. M., Loonstra, E. H., & Limburg, J. (2010). *Gamma-ray sensor for topsoil mapping; the Mole* (p. 10). The Medusa Institute. https://the.medusa.institute/display/GW/Publications

Wong, M. T. F., & Harper, R. J. (1999). Use of on-ground gamma-ray spectrometry to measure plant-available potassium and other topsoil attributes. *Soil Research*, *37*(2), 267. https://doi.org/10.1071/S98038

Yan, L., & Roy, D. P. (2016). Conterminous United States crop field size quantification from multi-temporal Landsat data. *Remote Sensing of Environment*, *172*, 67–86. https://doi.org/10.1016/j.rse.2015.10.034

Zreda, M., Desilets, D., Ferré, T. P. A., & Scott, R. L. (2008). Measuring soil moisture content non-invasively at intermediate spatial scale using cosmic-ray neutrons. *Geophysical Research Letters*, *35*(21), L21402. https://doi.org/10.1029/2008GL035655

Zreda, M., Shuttleworth, W. J., Zeng, X., Zweck, C., Desilets, D., Franz, T., & Rosolem, R. (2012). COSMOS: The COsmic-ray Soil Moisture Observing System. *Hydrology and Earth System Sciences*, *16*(11), 4079–4099. https://doi.org/10.5194/hess-16-4079-2012

CHAPTER 3

FUTURE RESEARCH

3.1 Introduction

In chapter three I expound on the future work that can be done to address: 1) a systematic understanding of sensor performance in specific conditions and 2) the value of proximal soil sensing to the agriculture industry. Chapter two reported sensor performance in three sandy parent material settings in North Dakota, as well as the feasibility of soil mapping with only 15 soil samples per 50 ha. Future work involves both new data collection and synthesis of the data already available from peer reviewed literature, extension offices, and precision agriculture dealers. Specifically, future studies can streamline decision making by demonstrating conceptual understandings of sensor best use, cost-benefit analysis, and optimal soil sampling strategies.

3.2 Best use

First, future soil mapping for precision management requires a more complete framework of the contexts in which each sensor is most appropriate. “Best use” describes the specific conditions in which a sensor most successfully predicts soil properties and discriminates between different soil management zones. When choosing the best geophysical sensor, conditions such as parent mineralogy, texture, organic matter content, soil depth, salinity, and soil moisture should all be accounted for (Doolittle & Brevik, 2014; Priori et al., 2014). Prior knowledge of the target soil property’s in-field variability should also be considered because lack of spatial variability will render a soil map of that target property meaningless for variable management. A decision flow chart for sensor

selection can be developed where decisions are based on any prior knowledge of the field conditions, such as data from the SSURGO soil data base (Soil Survey Staff, 2021).

Development of a systematic conceptual framework of best use would be possible through synthesis of the current literature and exploration of physically based models for sensor responses. Physically based models of sensor response would describe the impact of different field conditions on sensor performance. If the estimated sensor response has negligible spatial variability, the sensor may not be the best to use for differentiation of management zones within the given field. Current literature on EMI sensing allows some inferences to be made about the potential performance of EMI in different salinity, texture, soil depth, temperature, and soil moisture conditions (Adamchuk, Hummel, et al., 2004b; Doolittle & Brevik, 2014; A. B. McBratney et al., 2005). Visconti and De Paz (2021) were the first to develop a physically based, semi-empirical model for EMI measurements. They modeled depth-weighted apparent bulk electrical conductivity as a function of salinity, soil water content, clay, organic matter, bulk density, and temperature. In external validation of the EMI response model, Visconti and De Paz found R^2 of 0.8 for vertical dipole orientation and R^2 of 0.9 in the horizontal dipole orientation (Visconti & De Paz, 2021).

In contrast to the major drivers of EMI response, physical models of GRS response would likely be heavily reliant on parent mineralogy (Priori et al., 2014) and also be affected to a lesser degree by other properties such as soil texture, soil water content, organic matter, and pH (Dierke & Werban, 2013; IAEA, 2003; Megumi & Mamuro, 1977). Despite the evidence that site-specific calibrations are required for mapping with GRS (Rodrigues Jr. et al., 2015; Wong & Harper, 1999), at least one study suggests that

it may be possible to develop a generalized prediction of GRS response using non-linear functions (Heggemann et al., 2017). Heggemann et al. (2017) employed support vector machine methods to calibrate a soil texture model using GRS for ten different arable fields in Germany and achieved an average mean absolute error of prediction at all the sites of less than 5% sand, silt, or clay.

The variability in CRNS response can be estimated by prior knowledge of texture or soil hydraulic properties since repeat CRNS surveys have successfully mapped soil hydraulic properties (Finkenbiner et al., 2019; Gibson & Franz, 2018). Once the physical processes that affect EMI, GRS and CRNS are better understood, sensitivity analyses can be run on physically based models to simulate sensor performance in a variety of field conditions. Monte Carlo simulations of GRS and CRNS detector response are also a successful option for sensitivity analyses of changing environmental variables (Baldoncini et al., 2018; de Groot et al., 2009; Franz et al., 2012). Establishment of physically based models for sensor responses will allow users to make decisions of whether or not to conduct a specific survey based on known field conditions.

3.3 Cost-benefit analysis

In addition to better understanding the best use of each sensor on a conceptual level, the precision agriculture industry will benefit from decision-making tools based on cost-benefit analysis. Chapter two, for instance, could be extended into a site-specific cost-benefit analysis that bridges the feasibility gap between research and application. This would require quantification of error propagation in the soil mapping method,

determination of sampling and analysis cost, and estimation of economic value added by each map.

A first step is to compare the tradeoff between cost of specific surveys and the accuracy of the soil maps obtained from those surveys. Chatterjee et al. published an analysis of data fusion with different combinations of proximal x-ray fluorescence (pXRF), visible-near infrared (vis-NIR), EMI, digital elevation model (DEM), and remote sensing data that can serve as a template for comparisons of cost versus accuracy (Chatterjee et al., 2021). Empirical cost-benefit analysis following Chatterjee et al. can provide accessible tools such as Figure 3.1, which compares proximal sensing with EMI, GRS, and CRNS. In addition to accuracy, a cost-benefit analysis must also evaluate quality of predictions (Malone et al., 2011). Malone et al. (2011) introduced two quality measures with which users can consider the width of the prediction interval and how often the true soil property value lies within the prediction interval. Finally, a cost-benefit analysis should culminate in estimating profitability per acre. Profitability per acre can be obtained by running yield models given the field conditions, planned management inputs, and uncertainty (Bennett et al., 2021).

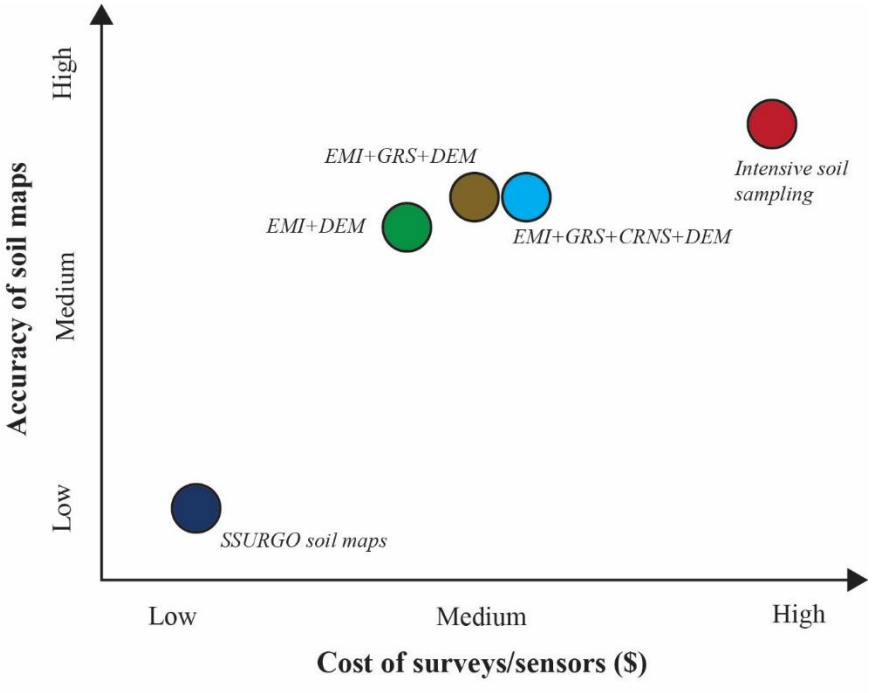

Figure 3.1. Potential results of a future cost-benefit analysis of soil mapping methods with proximal sensors for the top 30 cm of the soil profile. Electromagnetic induction (EMI), digital elevation models (DEM), gamma-ray sensing (GRS), cosmic-ray neutron sensing (CRNS), Soil Survey Geographic Database (SSURGO), and intensive soil sampling (one sample/ha) are compared. Concept is adapted from Figure 9 in Chatterjee et al., 2021.

3.4 Optimize soil sampling

Besides tradeoffs between technology costs, accuracy, and profitability, another sub-category of the cost-benefit analysis is optimization of soil sampling. Both the number and locations of soil samples should be optimized to achieve greatest map value with lowest time and labor costs. Various studies have sought to optimize soil sample locations and required number of soil samples (Brus, 2021; Ramirez-Lopez et al., 2019; Van Arkel & Kaleita, 2014) but there isn't a best universal sampling method. Optimization is unique for each soil mapping context given the mapping goals, field conditions, and performance of the soil sensors chosen. In a study on pH mapping for lime application, Adamchuk, Morgan et al. (2004) et al. modeled the net return over cost

of liming for various sampling and lime application strateges. The model was a function of cost and error of each mapping technique, mean and covariance function of the true soil pH, cost of lime application, yield response to prescribed lime application rate, and price of crops. A sensitivity analysis evaluated each mapping strategy over a range of initial field conditions and crop prices. Chapter two proposed k-means clustering of SSURGO and elevation data for sample location selection. This strategy can be compared to other sampling methodologies via a sensitivity analysis in a simulated random field following Adamchuk, Morgan, et al (2004).

3.5 Conclusions

Chapter one outlined the need for 1) a systematic understanding of sensor performance in specific conditions and 2) the value of proximal soil sensing to the agriculture industry. Chapter two addressed these concerns by providing results of soil mapping with geophysical sensors at three new settings in North Dakota, United States. Site-specific soil property predictions met precision management uncertainty targets at two of the three sites. The future of soil mapping for precision management with geophysical sensors lies in development of physically based understanding of sensors' best use, sophisticated cost-benefit analysis, and soil sampling optimization.

References

Abdu, H., Robinson, D. A., & Jones, S. B. (2007). Comparing Bulk Soil Electrical Conductivity Determination Using the DUALEM-1S and EM38-DD Electromagnetic Induction Instruments. *Soil Science Society of America Journal*, *71*(1), 189–196. https://doi.org/10.2136/sssaj2005.0394

Adamchuk, V. I., Hummel, J. W., Morgan, M. T., & Upadhyaya, S. K. (2004a). On-the-go soil sensors for precision agriculture. *Computers and Electronics in Agriculture*, *44*(1), 71–91. https://doi.org/10.1016/j.compag.2004.03.002

Adamchuk, V. I., Hummel, J. W., Morgan, M. T., & Upadhyaya, S. K. (2004b). On-the-go soil sensors for precision agriculture. *Computers and Electronics in Agriculture*, *44*(1), 71–91. https://doi.org/10.1016/j.compag.2004.03.002

Adamchuk, V. I., Morgan, M. T., & Lowenberg-Deboer, J. M. (2004). A Model for Agro-Economic Analysis of Soil pH Mapping. *Precision Agriculture*, *5*(2), 111–129. https://doi.org/10.1023/B:PRAG.0000022357.28154.eb

Andreasen, M., Jensen, K. H., Desilets, D., Franz, T. E., Zreda, M., Bogena, H. R., & Looms, M. C. (2017). Status and Perspectives on the Cosmic-Ray Neutron Method for Soil Moisture Estimation and Other Environmental Science Applications. *Vadose Zone Journal*, *16*(8), vzj2017.04.0086. https://doi.org/10.2136/vzj2017.04.0086

Andreasen, M., Jensen, K. H., Zreda, M., Desilets, D., Bogena, H., & Looms, M. C. (2016). Modeling cosmic ray neutron field measurements: MODELING COSMIC RAY NEUTRON FIELD MEASUREMENTS. *Water Resources Research*, *52*(8), 6451–6471. https://doi.org/10.1002/2015WR018236

Baldoncini, M., Albéri, M., Bottardi, C., Chiarelli, E., Kassandra Giulia Cristina Raptisa, Strati, V., & Mantovani, F. (2019). Biomass water content effect on soil moisture assessment via proximal gamma-ray spectroscopy. *Geoderma*, *335*, 69–77.

Baldoncini, M., Albéri, M., Chiarelli, E., Giulia Cristina Raptisa, K., Strati, V., & Mantovani, F. (2018). Investigating the potentialities of Monte Carlo simulation for assessing soil water content via proximal gamma-ray spectroscopy. *Journal of Environmental Radioactivity*, *192*, 105–116.

Bennett, J. McL., Roberton, S. D., Ghahramani, A., & McKenzie, D. C. (2021). Operationalising soil security by making soil data useful: Digital soil mapping, assessment and return-on-investment. *Soil Security*, *4*, 100010. https://doi.org/10.1016/j.soisec.2021.100010

Bottardi, C., Albéri, M., Baldoncini, M., Chiarelli, E., Montuschi, M., Raptis, K. G. C., Serafini, A., Strati, V., & Mantovani, F. (2020). Rain rate and radon daughters' activity. *Atmospheric Environment*, *238*, 117728. https://doi.org/10.1016/j.atmosenv.2020.117728

Brus, D. J. (2019). Sampling for digital soil mapping: A tutorial supported by R scripts. *Geoderma*, *338*, 464–480. https://doi.org/10.1016/j.geoderma.2018.07.036

Brus, D. J. (2021). Statistical approaches for spatial sample survey: Persistent misconceptions and new developments. *European Journal of Soil Science*, *72*(2), 686–703. https://doi.org/10.1111/ejss.12988

Caciolli, A., Baldoncini, M., Bezzon, G. P., Broggini, C., Buso, G. P., Callegari, I., Colonna, T., Fiorentini, G., Guastaldi, E., Mantovani, F., Massa, G., Menegazzo, R., Mou, L., Rossi Alvarez, C., Shyti, M., Zanon, A., & Xhixha, G. (2012). A new

FSA approach for in situ γ ray spectroscopy. *Science of the Total Environment*, *414*, 639–645.

Carroll, T. R. (1981). AIRBORNE SOIL MOISTURE MEASUREMENT USING NATURAL TERRESTRIAL GAMMA RADIATION: *Soil Science*, *132*(5), 358–366. https://doi.org/10.1097/00010694-198111000-00006

Castrignanò, A., Buttafuoco, G., Quarto, R., Parisi, D., Viscarra Rossel, R. A., Terribile, F., Langella, G., & Venezia, A. (2018). A geostatistical sensor data fusion approach for delineating homogeneous management zones in Precision Agriculture. *CATENA*, *167*, 293–304. https://doi.org/10.1016/j.catena.2018.05.011

Castrignanò, A., Wong, M. T. F., Stelluti, D., De Benedetto, D., & Sollitto, D. (2012). Use of EMI, gamma-ray emission and GPS height as multi-sensor data for soil characterisation. *Geoderma*, *175–176*, 78–89. http://dx.doi.org/10.1016/j.geoderma.2012.01.013

Chatterjee, S., Hartemink, A. E., Triantafilis, J., Desai, A. R., Soldat, D., Zhu, J., Townsend, P. A., Zhang, Y., & Huang, J. (2021). Characterization of field-scale soil variation using a stepwise multi-sensor fusion approach and a cost-benefit analysis. *CATENA*, *201*, 105190. https://doi.org/10.1016/j.catena.2021.105190

de Groot, A. V., van der Graaf, E. R., de Meijer, R. J., & Maučec, M. (2009). Sensitivity of in-situ γ-ray spectra to soil density and water content. *Nuclear Instruments and Methods in Physics Research Section A: Accelerators, Spectrometers, Detectors and Associated Equipment*, *600*(2), 519–523. https://doi.org/10.1016/j.nima.2008.12.003

Dierke, C., & Werban, U. (2013). Relationships between gamma-ray data and soil properties at an agricultural test site. *Geoderma*, *199*, 90–98. https://doi.org/10.1016/j.geoderma.2012.10.017

Doolittle, J. A., & Brevik, E. C. (2014). The use of electromagnetic induction techniques in soils studies. *Geoderma*, *223–225*, 33–45. https://doi.org/10.1016/j.geoderma.2014.01.027

Evett, S. R., O'Shaughnessy, S. A., Andrade, M. A., Kustas, W. P., Anderson, M. C., Schomberg, H. H., & Thompson, A. (2020). Precision Agriculture and Irrigation: Current U.S. Perspectives. *Transactions of the ASABE*, *63*(1), 57–67. https://doi.org/10.13031/trans.13355

Finkenbiner, C. E., Franz, T. E., Gibson, J., Heeren, D. M., & Luck, J. (2019). Integration of hydrogeophysical datasets and empirical orthogonal functions for improved irrigation water management. *Precision Agriculture*, *20*(1), 78–100. https://doi.org/10.1007/s11119-018-9582-5

Florinsky, I. V., Eilers, R. G., Manning, G. R., & Fuller, L. G. (2002). Prediction of soil properties by digital terrain modelling. *Environmental Modelling and Software*, *17*(3), 295–311. https://doi.org/10.1016/S1364-8152(01)00067-6

Franz, T. E., Zreda, M., Ferre, T. P. A., Rosolem, R., Zweck, C., Stillman, S., Zeng, X., & Shuttleworth, W. J. (2012). Measurement depth of the cosmic ray soil moisture probe affected by hydrogen from various sources: MEASUREMENT DEPTH OF THE COSMIC-RAY SOIL MOISTURE PROBE. *Water Resources Research*, *48*(8). https://doi.org/10.1029/2012WR011871

Franz, T. E., Zreda, M., Rosolem, R., Hornbuckle, B. K., Irvin, S. L., Adams, H., Kolb, T. E., Zweck, C., & Shuttleworth, W. J. (2013). Ecosystem-scale measurements of biomass water using cosmic ray neutrons: ECOSYSTEM MEASUREMENTS OF BIOMASS WATER. *Geophysical Research Letters*, *40*(15), 3929–3933. https://doi.org/10.1002/grl.50791

Gibson, J., & Franz, T. E. (2018). Spatial prediction of near surface soil water retention functions using hydrogeophysics and empirical orthogonal functions. *Journal of Hydrology*, *561*, 372–383. https://doi.org/10.1016/j.jhydrol.2018.03.046

Grasty, R. L. (1997). Radon emanation and soil moisture effects on airborne gamma-ray measurements. *Geophysics*, *62*(5), 1379–1385.

Grunwald, S., Vasques, G. M., & Rivero, R. G. (2015). Fusion of Soil and Remote Sensing Data to Model Soil Properties. In *Advances in Agronomy* (Vol. 131, pp. 1–109). Elsevier. https://doi.org/10.1016/bs.agron.2014.12.004

Heggemann, T., Welp, G., Amelung, W., Angst, G., Franz, S. O., Koszinski, S., Schmidt, K., & Pätzold, S. (2017). Proximal gamma-ray spectrometry for site-independent in situ prediction of soil texture on ten heterogeneous fields in Germany using support vector machines. *Soil and Tillage Research*, *168*, 99–109. https://doi.org/10.1016/j.still.2016.10.008

Hendriks, P. H. G. M., Limburg, J., & de Meijer, R. J. (2001). Full-spectrum analysis of natural γ-ray spectra. *Journal of Environmental Radioactivity*, *53*(3), 365–380. https://doi.org/10.1016/S0265-931X(00)00142-9

IAEA. (2003). *Guidelines for radio element mapping using gamma ray spectrometry data* (No. 1363; Technical Documents). International Atomic Energy Agency.

Ji, W., Adamchuk, V. I., Chen, S., Biswas, A., Mat Su, A. S., Ismail, A., Gan, Q., & Shi, Z. (2019). Simultaneous measurement of multiple soil properties through proximal sensor data fusion: A case study. *Geoderma*, *341*, 111–128.

Jiménez-Jiménez, S. I., Ojeda-Bustamante, W., Marcial-Pablo, M., & Enciso, J. (2021). Digital Terrain Models Generated with Low-Cost UAV Photogrammetry: Methodology and Accuracy. *ISPRS International Journal of Geo-Information*, *10*(5), 285. https://doi.org/10.3390/ijgi10050285

Köhli, M., Schrön, M., Zreda, M., Schmidt, U., Dietrich, P., & Zacharias, S. (2015). Footprint Characteristics Revised for Field-Scale Soil Moisture Monitoring with Cosmic-Ray Neutrons. *Water Resources Research*, *51*(7), 5772–5790. https://doi.org/10.1002/2015WR017169

Lowenberg-DeBoer, B. E. | J. (2017, June 1). 2017 Precision Dealership Survey: Making the Turn Toward Decision Agriculture. *CropLife*. https://www.croplife.com/iron/2017-precision-dealership-survey-making-the-turn-toward-decision-agriculture/

Mahmood, H. S. M., Hoogmoed, W. B., & van Henten, E. J. (2013). Proximal Gamma-Ray Spectroscopy to Predict Soil Properties Using Windows and Full-Spectrum Analysis Methods. *Sensors*, *13*, 16263–16280. https://doi.org/10.3390/s131216263

Malone, B. P., de Gruijter, J. J., McBratney, A. B., Minasny, B., & Brus, D. J. (2011). Using Additional Criteria for Measuring the Quality of Predictions and Their Uncertainties in a Digital Soil Mapping Framework. *Soil Science Society of America Journal*, *75*(3), 1032–1043. https://doi.org/10.2136/sssaj2010.0280

McBratney, A. B., Minasny, B., & Whelan, B. M. (2005). Obtaining 'useful' high-resolution soil data from proximally-sensed electrical conductivity/resistivity (PSEC/R) Surveys. In J. V. Stafford (Ed.), *Precision Agriculture '05: Proceedings of the 5th European Conference on Precision Agriculture*. Wageningen Academic Publishers. https://doi.org/10.3920/978-90-8686-549-9

McBratney, A., Minasny, B., & Whelan, B. M. (2005). Obtaining 'useful' high-resolution soil data from proximally-sensed electrical conductivity/resistivity (PSEC/R) surveys. In J. V. Stafford (Ed.), *Precision Agriculture '05* (pp. 503–510). Wageningen Academic Publishers.

Megumi, K., & Mamuro, T. (1977). Concentration of uranium series nuclides in soil particles in relation to their size. *Journal of Geophysical Research*, *82*(2), 353–356. https://doi.org/10.1029/JB082i002p00353

Morris, E. R. (2009). Height-above-ground effects on penetration depth and response of electromagnetic induction soil conductivity meters. *Computers and Electronics in Agriculture*, *68*(2), 150–156. https://doi.org/10.1016/j.compag.2009.05.009

Polidori, L., & El Hage, M. (2020). Digital Elevation Model Quality Assessment Methods: A Critical Review. *Remote Sensing*, *12*(21), 3522. https://doi.org/10.3390/rs12213522

Priori, S., Bianconi, N., & Costantini, E. A. C. (2014). Can γ-radiometrics predict soil textural data and stoniness in different parent materials? A comparison of two machine-learning methods. *Geoderma*, *226–227*, 354–364. https://doi.org/10.1016/j.geoderma.2014.03.012

Ramirez-Lopez, L., Wadoux, A. M. J. -C., Franceschini, M. H. D., Terra, F. S., Marques, K. P. P., Sayão, V. M., & Demattê, J. A. M. (2019). Robust soil mapping at the farm scale with vis–NIR spectroscopy. *European Journal of Soil Science*, *70*(2), 378–393. https://doi.org/10.1111/ejss.12752

Rodrigues Jr., F. A., Bramley, R. G. V., & Gobbett, D. L. (2015). Proximal soil sensing for Precision Agriculture: Simultaneous use of electromagnetic induction and gamma radiometrics in contrasting soils. *Geoderma*, *243–244*, 183–195. http://dx.doi.org/10.1016/j.geoderma.2015.01.004

Rossel, R. A. V., Taylor, H. J., & McBratney, A. B. (2007). Multivariate calibration of hyperspectral γ-ray energy spectra for proximal soil sensing. *European Journal of Soil Science*, *58*(1), 343–353. https://doi.org/10.1111/j.1365-2389.2006.00859.x

Schimmelpfennig, D. (Ed.). (2016). *Farm Profits and Adoption of Precision Agriculture*. https://doi.org/10.22004/ag.econ.249773

Söderstrom, M., Sohlenius, G., Rodhe, L., & Piikki, K. (2016). Adaptation of regional digital soil mapping for precision agriculture. *Precision Agriculture*, *17*, 588–607.

Soil Survey Staff, Natural Resources Conservation Service, United States Department of Agriculture. Web Soil Survey. Available at https://websoilsurvey.nrcs.usda.gov/. (verified 5 April 2021).

Taylor, J. A., Short, M., McBratney, A. B., & Wilson, J. (2010). Comparing the Ability of Multiple Soil Sensors to Predict Soil Properties in a Scottish Potato Production System. In R. A. Viscarra Rossel, A. B. McBratney, & B. Minasny (Eds.), *Proximal Soil Sensing* (pp. 387–396). Springer Netherlands. https://doi.org/10.1007/978-90-481-8859-8_33

Triantafilis, J., & Lesch, S. M. (2005). Mapping clay content variation using electromagnetic induction techniques. *Computers and Electronics in Agriculture*, *46*(1–3), 203–237. https://doi.org/10.1016/j.compag.2004.11.006

Van Arkel, Z., & Kaleita, A. L. (2014). Identifying sampling locations for field-scale soil moisture estimation using K-means clustering. *Water Resources Research*, *50*(8), 7050–7057. https://doi.org/10.1002/2013WR015015

van der Klooster, E., van Egmond, F. M., & Sonneveld, M. P. W. (2011). Mapping soil clay contents in Dutch marine districtsusing gamma-ray spectrometry. *European Journal of Soil Science*, *62*(5), 743–753.

van der Veeke, S., Limburg, J., Koomans, R. L., Söderström, M., de Waal, S. N., & van der Graaf, E. R. (2021). Footprint and height corrections for UAV-borne gamma-ray spectrometry studies. *Journal of Environmental Radioactivity*, *231*. https://doi.org/10.1016/j.jenvrad.2021.106545

van Egmond, F. M., Loonstra, E. H., & Limburg, J. (2010). *Gamma-ray sensor for topsoil mapping; the Mole* (p. 10). The Medusa Institute. https://the.medusa.institute/display/GW/Publications

Viscarra Rossel, R. A., Cattle, S. R., Ortega, A., & Fouad, Y. (2009). In situ measurements of soil colour, mineral composition and clay content by vis–NIR spectroscopy. *Geoderma*, *150*(3–4), 253–266. https://doi.org/10.1016/j.geoderma.2009.01.025

Visconti, F., & De Paz, J. M. (2021). A semi-empirical model to predict the EM38 electromagnetic induction measurements of soils from basic ground properties. *European Journal of Soil Science*, *72*(2), 720–738. https://doi.org/10.1111/ejss.13044

Wong, M. T. F., & Harper, R. J. (1999). Use of on-ground gamma-ray spectrometry to measure plant-available potassium and other topsoil attributes. *Soil Research*, *37*(2), 267. https://doi.org/10.1071/S98038

Wong, M. T. F., Oliver, Y. M., & Robertson, M. J. (2009). Gamma-Radiometric Assessment of Soil Depth across a Landscape Not Measurable Using Electromagnetic Surveys. *Soil Science Society of America Journal*, *73*(4), 1261–1267. https://doi.org/10.2136/sssaj2007.0429

Zhang, Y., Ji, W., Saurette, D. D., Easher, T. H., Li, H., Shi, Z., Adamchuk, V. I., & Biswas, A. (2020). Three-dimensional digital soil mapping of multiple soil properties at a field-scale using regression kriging. *Geoderma*, *366*, 114253. https://doi.org/10.1016/j.geoderma.2020.114253

Zhu, Y., Weindorf, D. C., & Zhang, W. (2011). Characterizing soils using a portable X-ray fluorescence spectrometer: 1. Soil texture. *Geoderma*, *167–168*, 167–177. https://doi.org/10.1016/j.geoderma.2011.08.010

Zreda, M., Desilets, D., Ferré, T. P. A., & Scott, R. L. (2008). Measuring soil moisture content non-invasively at intermediate spatial scale using cosmic-ray neutrons. *Geophysical Research Letters*, *35*(21), L21402. https://doi.org/10.1029/2008GL035655

Zreda, M., Shuttleworth, W. J., Zeng, X., Zweck, C., Desilets, D., Franz, T., & Rosolem, R. (2012). COSMOS: The COsmic-ray Soil Moisture Observing System. *Hydrology and Earth System Sciences*, *16*(11), 4079–4099. https://doi.org/10.5194/hess-16-4079-2012

APPENDIX

The supplemental R code and figures for each site analyzed in Chapter 2 is available online at: https://data.mendeley.com/datasets/vhm3xtsm72/2 .

The data used in the Chapter 2 analysis is available online at: https://data.mendeley.com/datasets/c2zb42vd4h/2 .